

## 7. SITE 1004<sup>1</sup>

### Shipboard Scientific Party<sup>2</sup>

#### HOLE 1004A

**Position:** 24°33.283'N, 79°14.95'W

**Start hole:** 1445 hr, 6 March 1996

**End hole:** 1815 hr, 7 March 1996

**Time on hole:** 1 day, 3 hr, 30 min

**Seafloor (drill pipe measurement from rig floor, mbrf):** 430.2

**Total depth (drill pipe measurement from rig floor, mbrf):** 630.2

**Distance between rig floor and sea level (m):** 11.3

**Water depth (drill pipe measurement from sea level, m):** 418.9

**Penetration (mbsf):** 200

**Coring totals:**

Type: APC; No: 12; Cored: 102.8 m; Recovered: 87.8%

Type: XCB; No: 11; Cored: 97.2 m; Recovered: 28.1%

**Formation:**

Unit I: 0–200 mbsf; Pleistocene to early Pliocene in age

Unlithified to partially lithified wackestones and mudstones with intercalations of coarser grained packstones and floatstones

**Principal results:** The primary objective of Site 1004 was to obtain heat flow and interstitial water geochemistry measurements to be used in conjunction with data obtained from Sites 1003, 1005, 1006, and 1007 to ascertain possible fluid flow and diagenetic reactions in the carbonate margin. In addition, this site serves as a location for the study of high-resolution sea-level changes during the Pleistocene and provides additional information for the sea-level objectives of Leg 166.

A Pliocene–Pleistocene section (200 m) was drilled at Site 1004 on the western slope of the Great Bahama Bank. The strata consist of a series of mixed pelagic and bank-derived carbonates, with a carbonate content of 92%–97%. Sediments of late Pliocene age are reached at the base of the core. Adara and WSTP temperature measurements confirm the presence of a nonsteady state temperature profile, suggesting an inflow of water into the slope sediments. Pore-water geochemistry and gas analyses show an extremely active diagenetic zone between 110 and 200 mbsf with alkalinity values as high as 70 mM, depletions in Mg<sup>2+</sup> and Ca<sup>2+</sup>, and enrichments in Sr<sup>2+</sup>. This zone has high concentrations of methane and hydrogen sulfide. Hydrogen sulfide readily degassed from the cores between 50 and 135 mbsf as soon as they were brought to the surface.

One major lithologic unit was distinguished:

Unit I (0–200 mbsf) is of Holocene to latest Pliocene age and is equivalent to Unit I described in Site 1003. It consists of several 5- to 10-m-thick intervals of light-colored, unlithified to partially lithified peloidal wackestones to mudstones that alternate with thin 0.5- to 1-m intervals of gray, partially lithified wackestones to packstones, grainstones, and floatstones. Subunit IA (0–81.1 mbsf) contains multiple oscillations between zones of coarse, blackened grains with lithoclasts and fine periplatform ooze. Subunit IB (81.1–200 mbsf) contains an overall coarsening-upward

sequence of partially dolomitized mudstones and wackestones with some coarser grained intervals.

Sediments recovered from Hole 1004A provide a record for the Pleistocene through the uppermost Pliocene, although the abundance and preservation of both nannofossils and foraminifers vary throughout the recovered sequence. The sedimentation rate is high throughout the Pleistocene, and modern platform production and shedding began to influence this site much earlier than the more distal site, Site 1003. Throughout Subunit IA, a number of alternations in sediment composition, color, and mineralogy can be recognized, probably corresponding to sea-level changes. Lowstands are characterized by higher concentration of low-magnesium calcite (LMC) and darker color compared to highstands, which contain abundant aragonite and high-magnesium calcite (HMC). Below the bottom of Subunit IA, these cycles can no longer be recognized as a result of poor core recovery and the influence of diagenesis, which results in the dissolution of aragonite and HMC and the formation of dolomite.

On the basis of pore-water geochemistry, two distinct geochemical zones have been identified within Site 1004. An upper zone, extending from the seafloor to a depth of 40 mbsf, is characterized by an absence of significant changes in the interstitial pore-water geochemistry. Geothermal measurements indicate a reduced temperature gradient in this interval, also suggesting the influx of seawater. The upper zone gradually merges into a region with salinity between 45 and 50, below 110 mbsf. In this lower region, concentrations of both Ca<sup>2+</sup> and Mg<sup>2+</sup> are depressed and Sr<sup>2+</sup> is elevated. This region corresponds to high concentrations of CH<sub>4</sub> (up to 20,000 ppm) and H<sub>2</sub>S (up to 21,000 ppm). Although the C<sub>1</sub>/C<sub>2</sub> ratio was over 2000 in this region, there were still detectable concentrations of C<sub>3</sub> and C<sub>4</sub> gases present.

### BACKGROUND AND OBJECTIVES

Site 1004 is located on the middle slope approximately 3 km from the western platform edge of the Great Bahama Bank (GBB) in 418.9 m of water (Fig. 1). The principal objective of drilling at Site 1004 was to determine the extent and mechanism of fluid flow in the margin of the GBB. A secondary objective was to examine, in conjunction with Sites 1003 and 1005, changes in sedimentation on the lower and middle slope of the western margin of the GBB and to date sequence boundaries, which could then be traced to Sites 1003 and 1005 (Fig. 2). The original target depth of Site 1004 was 250 mbsf, but drilling terminated at 200 mbsf when objectives were considered to be achieved.

It is postulated that fluid is actively moving through the sediments at the margin of the GBB. Two mechanisms have been proposed. One arises as a result of underpressure caused by temperature differences between the interior of the platform and the Straits of Florida. In the center portion of the platform, temperature gradually increases with depth, whereas at a corresponding depth in the Straits of Florida, the temperature is considerably colder. This temperature difference causes the water in the platform interior to rise, causing water to enter through the sides of the platform. This mechanism has been described and documented in Florida and has been termed “Kohout convection” (Kohout, 1966, 1967). A second mechanism whereby fluids might be circulated through the platform results from the reflux of more saline waters derived on the surface of the Great Bahama Bank. These fluids by virtue of their greater density would sink through the

<sup>1</sup>Eberli, G.P., Swart, P.K., Malone, M.J., et al., 1997. *Proc. ODP, Init. Repts.*, 166: College Station, TX (Ocean Drilling Program).

<sup>2</sup>Shipboard Scientific Party is given in the list preceding the Table of Contents.

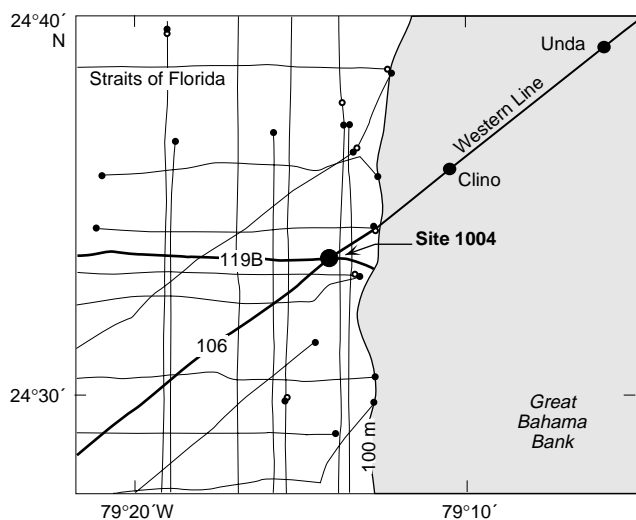


Figure 1. Location map of Site 1004. The site is located on the same seismic line as the two drill sites Unda and Clino that were drilled from a self-propelled jack-up barge on the shallow top of the Great Bahama Bank in a water depth of 7 m.

platform preferentially flowing through the more permeable strata. These mechanisms possibly provide fluids with diagenetic potential to alter the metastable sediments produced on the platform and subsequently deposited on the slope to LMC and dolomite. To test the Kohout convection and reflux model, a series of closely spaced holes (1003, 1004, and 1005) was drilled as close as possible to the platform margin as allowed by the current ODP safety regulations. Evidence of fluid flow was postulated to be present as nonsteady state geothermal and geochemical gradients. Temperature measurements were made on every core using the Adara tool from Core 4H to APC refusal and thereafter using the WSTP tool every third core. Samples for interstitial water chemistry were taken every other section over the upper three cores and on every third core thereafter.

## OPERATIONS

### Hole 1004A

The ship was moved 0.8 nmi from the location of Hole 1003C to the GPS coordinates for Site 1004 at 24°33.283'N, 79°14.95'W. A beacon was dropped and coring at Hole 1004A was initiated at 2010 hr on 6 March. The water depth was 418.9 mbsl based on recovery of the mudline core. APC Cores 1H through 12H were cut from 0 to 102.8 mbsf with recovery ranging from 2.1% to 103% (mean = 87.8%) (Table 1). Cores 3H–7H and 9H–11H were oriented, and Adara heat flow measurements were performed at Cores 4H through 8H, 10H, and 12H. Recovery was reduced by hard layers jamming in the throat of the bit, and thereafter, we switched to the XCB coring system. XCB Cores 13X through 23X were cut from 102.8 to 200 mbsf with recovery varying from 0 to 82.8% (mean = 28.1%). Coring was terminated when objectives for Site 1004 were achieved, and the bit cleared the seafloor at 1815 hr on 7 March.

## LITHOSTRATIGRAPHY

### Introduction

A 200-m sequence of Quaternary to upper Pliocene carbonate sediments was recovered from one hole drilled at Site 1004. Core recovery of the upper 93 m of Hole 1004A was nearly continuous. This interval consists of Pleistocene-aged unlithified to partially lithified peloidal wackestones and mudstones with intercalations of coarser

grained packstones and floatstones. Some nannofossil ooze to chalk also occurs in the upper 93 m of the hole. Facies are arranged in distinct depositional cycles within much of this upper interval. Recovery was moderate to poor below 93 mbsf, where lower Pleistocene to upper Pliocene mudstone, wackestone, packstone, and floatstone was encountered. These lithologies are only partially lithified in many intervals. Dolomite was observed in several cores below 116 mbsf (Section 166-1004A-12X-CC). The carbonate content at Site 1004 varies from 90% to 96% (see “Organic Geochemistry” section, this chapter).

## Description of Units

### Lithologic Unit I

Interval: 166-1004A-1H through 23X  
Age: Pleistocene to late Pliocene  
Depth: 0–200 mbsf

The entire sedimentary section recovered in Site 1004 corresponds to Unit I, defined previously at Site 1003, based on the presence of peloids (Fig. 3). As observed at Site 1003, Unit I can be divided into Subunits IA and IB. At Site 1004, Subunit IA is characterized by multiple alternations between zones of fine periplatform ooze (*sensu* Schlager and James, 1978) and intervals that contain coarse, blackened grains and/or lithoclasts. Bioturbation in Subunit IA is moderate to strong, and sedimentary structures are not present. Subunit IB contains mudstones and wackestones with several coarser grained floatstone and packstone intervals. Partially lithified mudstones, wackestones, and packstones also occur. The percentage of mud in the matrix decreases upward in both subunits. The boundary between Subunits IA and IB is placed at the base of a nannofossil ooze to chalk bed at Section 166-1004A-10H-4, 30 cm (81.1 mbsf).

### Lithologic Subunit IA

Interval: 166-1004A-1H through 10H-4, 30 cm  
Age: Pleistocene  
Depth: 0–81.1 mbsf

Subunit IA consists of 2- to 18-m-thick intervals of light-colored, unlithified to partially lithified peloidal wackestones to mudstones that alternate with 0.5- to 1-m-thick intervals of gray, partially lithified wackestones to packstones, grainstones, and floatstones. The thick, unlithified wackestones and partially lithified wackestones to mudstones are typical periplatform oozes consisting of peloids, planktonic and benthic foraminifers, and pteropods in a matrix of aragonite needles, micrite, and calcareous nannofossils. Grain size is bimodal throughout most of the periplatform ooze with grain sizes of silt to very fine sand and medium to coarse sand. The silt- to fine sand-sized fractions are well sorted. Peloids, benthic foraminifers, and subangular bioclasts are the dominant fine-grained allochems. Tunicate spicules and intraclasts were observed in smear slides. Coarse-grained allochems include planktonic and benthic foraminifers, echinoderm spines, gastropods, bivalves, and peloids. The coarse-grained, gray intervals consist of blackened grains often associated with large (0.5–5 cm), cemented and bored lithoclasts. Blackened grains include foraminifers, pteropod casts, gastropods, bivalves, and shell fragments.

In Subunit IA, the facies are arranged in seven depositional cycles (Fig. 4). Each cycle can be divided into three parts. The base of each cycle, with the exception of Cycle 7, is marked by an interval or layer that contains blackened grains and/or lithoclasts. The second part of the cycle consists of an upward increase in whitish (5Y 8/1 to 5Y 7/1) periplatform ooze with aragonite needles and micrite as the dominant matrix constituents. The third and upper part of each cycle is characterized by a decrease in aragonite needles and micrite and an increase in calcareous nannofossils in the matrix. The change in matrix composition from aragonite and micrite to nannofossils coincides with a gradational color change from white (5Y 8/1 to 5Y 7/1) to pale yellow (5Y 8/2) or light gray (2.5Y 7/2).

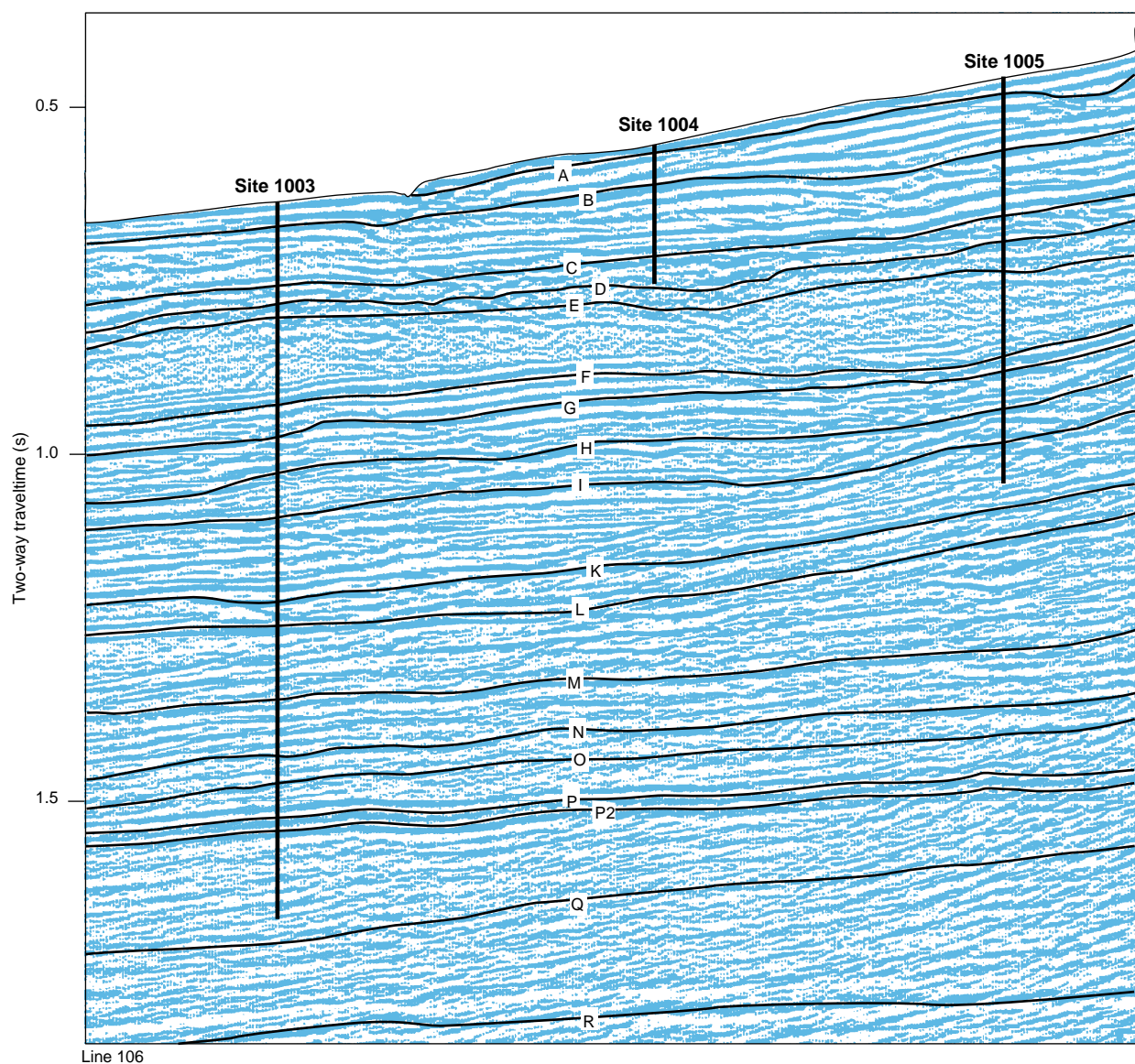


Figure 2. Interpreted seismic section connecting Sites 1005, 1004, and 1003.

Depositional variations identified in the visual core descriptions and smear-slide analyses are evident in percent color reflectance, XRD aragonite (see “Inorganic Geochemistry” section, this chapter), and natural gamma-ray data (see “Physical Properties” section, this chapter) (Fig. 4). Gray intervals with blackened grains and lithoclasts have low color reflectance (<40%, at 700 nm), aragonite- and micrite-rich intervals have high color reflectance (>55%, at 700 nm), and nannofossil-rich sediments are characterized by intermediate color reflectance (45%–55%, at 700 nm). High color reflectance correlates to high percent aragonite from XRD and low natural gamma-ray values. Low color reflectance correlates to low percent aragonite from XRD and high natural gamma-ray values.

#### Lithologic Subunit IB

Interval: 166-1004A-10H-3, 30 cm, through 23X  
Age: Pleistocene to late Pliocene  
Depth: 81.1–200 mbsf

Subunit IB consists of fine-grained peloidal mudstones, wackestones, packstones, and one floatstone interval. Some of these sediments are only partially lithified. The dominant lithology throughout this subunit is formed by sediments with a mudstone texture. In addition

to peloids, planktonic and benthic foraminifers occur throughout most of Subunit IB, but they are often difficult to identify as a result of poor preservation. Minor amounts of dolomite (up to 25% of the carbonate fraction) occur in this interval, as identified in smear slides and confirmed by XRD analysis (see “Inorganic Geochemistry” section, this chapter).

The interval from Section 166-1004A-10H-4, 30 cm, through Core 166-1004A-13X represents a transition between Subunit IA dominated by unlithified to partially lithified wackestones, with lithoclast and blackened grain layers above, and wackestone, mudstone and partially lithified wackestone, mudstone, and packstone layers below. No sedimentary structures are observed in this transitional interval. A downward increase in aragonite needles and micrite occurs within the upper part of the interval. Micrite decreases below Section 166-1004A-11H-1, 75 cm, and allochems are not preserved. The lower part of the transition interval consists of a slightly dolomitized, partially lithified foraminifer wackestone with blackened grains and bioclasts (Section 166-1004A-12H-CC) and partially dolomitized mudstone (Core 166-1004A-13X). No sedimentary structures are present in the transition zone.

The sediments become more mud supported from Core 166-1004A-14X to the base of Hole 1004A. The upper part of this interval

**Table 1. Site 1004 coring summary.**

Core	Date (March 1996)	Time (UTC)	Depth (mbsf)	Length cored (m)	Length recovered (m)	Recovery (%)
166-1004A-						
1H	7	0115	0.0–5.3	5.3	5.27	99.4
2H	7	0200	5.3–14.8	9.5	9.64	101.0
3H	7	0230	14.8–24.3	9.5	9.84	103.0
4H	7	0315	24.3–33.8	9.5	9.39	98.8
5H	7	0355	33.8–43.3	9.5	9.67	102.0
6H	7	0435	43.3–52.8	9.5	9.93	104.0
7H	7	0515	52.8–62.3	9.5	9.2	96.8
8H	7	0620	62.3–66.8	4.5	0.53	11.8
9H	7	0715	66.8–76.3	9.5	9.89	104.0
10H	7	0835	76.3–85.8	9.5	9.36	98.5
11H	7	0900	85.8–93.3	7.5	7.29	97.2
12H	7	1005	93.3–102.8	9.5	0.2	2.1
13X	7	1120	102.8–107.5	4.7	0.27	5.7
14X	7	1205	107.5–116.6	9.1	7.54	82.8
15X	7	1255	116.6–126.0	9.4	0.4	4.3
16X	7	1410	126.0–135.4	9.4	6.22	66.2
17X	7	1630	135.4–144.4	9	1.12	12.4
18X	7	1720	144.4–153.4	9	5.99	66.5
19X	7	1750	153.4–162.4	9	0.3	3.3
20X	7	1915	162.4–171.8	9.4	0.21	2.2
21X	7	1940	171.8–181.2	9.4	0.0	0.0
22X	7	2045	181.2–190.6	9.4	5.23	55.6
23X	7	2115	190.6–200.0	9.4	0.0	0.0
Coring totals				200.0	117.49	58.7

Note: An expanded version of this coring summary table that includes lengths and depths of sections, location of whole-round samples, and comments on sampling disturbance is included on CD-ROM in the back pocket of this volume.

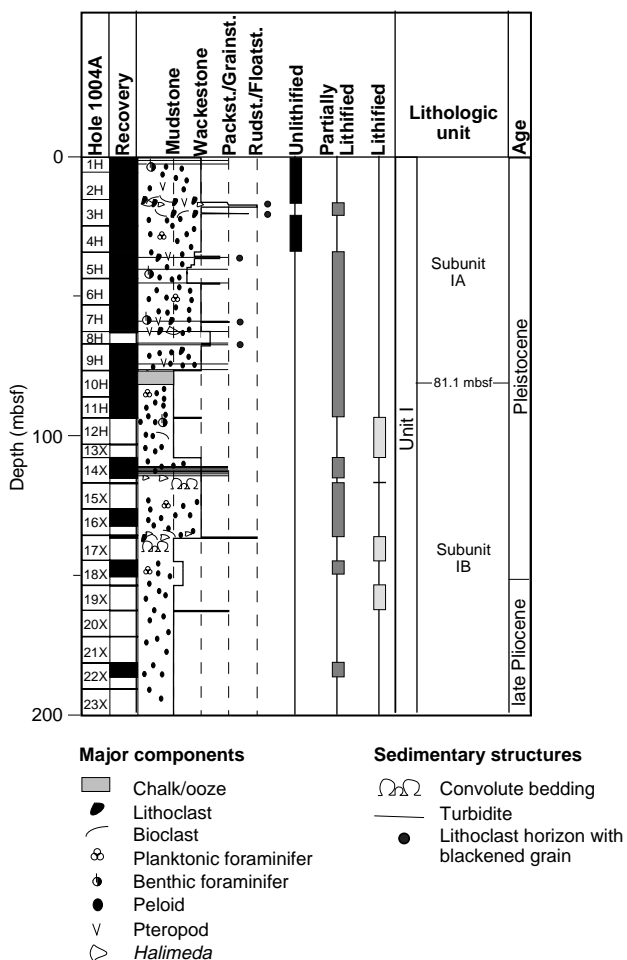


Figure 3. Lithologic summary for Site 1004.

consists of peloidal wackestone with numerous millimeter-scale planar laminations of packstone to grainstone layers. These thin layers consist of yellowish silt-sized and fine sand-sized tunicate spicules and foraminifers. Sets of laminae fine upward and range in thickness from 1 to 10 cm. A thin layer of *Halimeda* fragments (Section 166-1004A-14X-CC, 18 cm), directly overlying an interval of convolute bedding (Section 166-1004A-15X-CC), occurs just below the planar-laminated, fining-upward packstones.

A bioclastic floatstone occurs in interval 166-1004A-17X-1, 67–108 cm (Fig. 5). This floatstone contains *Halimeda* fragments, coral debris, red algae, bivalves, benthic foraminifers, and lithoclasts. Some of the skeletal grains are blackened. The interval has significant skeletal-moldic porosity with bladed to prismatic cements infilling dissolution voids. Convolute bedding occurs at the base of this interval. With the exception of a peloidal packstone in interval 166-1004A-20X, 0–20 cm, the remainder of Subunit IB consists of peloidal mudstones to wackestones and partially lithified peloidal mudstones to wackestones. A slight downcore decrease in peloids occurs below Core 166-1004A-20X in Subunit IB.

### Discussion

Depositional cycles observed in Subunit IA resemble periplatform aragonite cycles described in numerous piston cores from the slopes and deep basins surrounding the Bahama Banks (e.g., Kier and Pilkey, 1971; Droxler et al., 1983; Kenter, 1985; Slowey, 1985; Droxler et al., 1988). The major difference between aragonite cycles described in piston cores and those observed in Hole 1004A is the presence of large, cemented, and bored lithoclasts and numerous blackened grains. In addition, the large percentage of bank-derived peloids and benthic foraminifers found in Subunit IA of Hole 1004A is not typically observed in periplatform oozes recovered from deeper water settings located farther from the bank.

The well-established correlation between fine aragonite content and planktonic foraminifer  $\delta^{18}O$  values for Pleistocene periplatform oozes (Droxler et al., 1983, 1988) permits the preliminary interpretation of Site 1004 depositional cycles as glacial (lowstand) to interglacial (highstand) cycles. Intervals with lithoclasts and blackened grains (possible submarine hardgrounds) would correspond to lowstands in sea level, the sharp upward increase in aragonite needles and the decrease in aragonite needles and micrite and increase in calcareous nannofossils would correspond to the transition from sea-level highstands to lowstands. However, the presence of hiatuses within Subunit IA (see “Biostratigraphy” section, this chapter) makes it difficult to correlate aragonite cycles to specific late Quaternary oxygen isotope stages (SPECMAP; Imbrie et al., 1984).

The style of deposition in Subunit IB is different from that of Subunit IA. No regular variations in the matrix constituents or grain types are observed, although there is a downcore decrease in the mud-sized fraction below Core 166-1004A-14X. Two types of gravity deposits break up the monotonous background sedimentation of mud- and fine sand-sized pelagic and bank-derived material. A series of fining-upward sets of laminae (Core 166-1004A-14X) consisting of silt- and fine sand-sized foraminifers, tunicate spicules, and *Halimeda*, with convolute bedding at the base, may represent a period of platform-derived turbidite or grain flow deposition. A bioclastic floatstone consisting of *Halimeda*, coral debris, and red algae, with convolute bedding at the base, indicates the occurrence of a platform-margin-derived debris flow (Core 166-1004A-17X). The presence of blackened skeletal grains in this deposit indicate that it was probably formed during a relative sea-level lowstand.

### BIOSTRATIGRAPHY

Sediments recovered from Hole 1004A provide a record for the Pleistocene through the uppermost Pliocene. The abundances of cal-

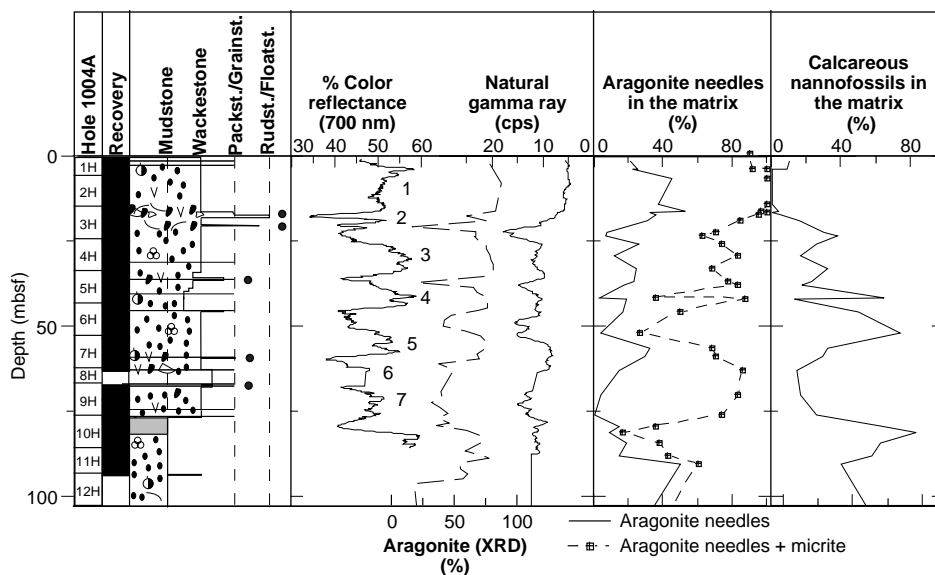


Figure 4. Lithology, percent color reflectance, natural gamma ray, percent aragonite from XRD, and matrix constituents (relative to total matrix) determined in smear slides. Depositional cycles are numbered 1 through 7. Note the good correlation between these data, particularly during depositional Cycles 1 through 5. High natural gamma-ray values in intervals of low color reflectance may result from elevated uranium concentrations in phosphatic, blackened grains.

careous nannofossils and foraminifers vary throughout the recovered sequence. Both groups are abundant and well preserved in the uppermost Pleistocene interval (Cores 166-1004A-1H and 2H). The preservation of nannofossils and planktonic foraminifers decreases markedly in Core 166-1004A-3H and remains poor to moderate through the rest of the hole (Core 166-1004A-22X). The Pliocene/Pleistocene boundary is placed at 152 mbsf between Samples 166-1004A-18X-CC and 19X-CC on the basis of nannofossils. The basal sediments are upper Pliocene. The Pliocene–Pleistocene section at Hole 1004A yields benthic foraminiferal faunas that indicate a paleodepth of ~200–500 m (within the upper bathyal zone). The preservation of the benthic fauna as well as the diversity of platform-derived species decreases in the lower Pleistocene to upper Pliocene interval.

### Calcareous Nannofossils

A total of 23 samples from Hole 1004A were examined for the distribution of calcareous nannofossil age-diagnostic species. Calcareous nannofossil datum levels are listed in Table 2 and shown in Figure 6. Calcareous nannofossils from this hole are moderately to poorly preserved except for the uppermost two samples, which are well preserved.

The first occurrence of *Emiliania huxleyi* defines the NN21/20 boundary (0.25 Ma) and is present in Sample 166-1004A-2H-CC. The base of NN21 is placed between Samples 166-1004A-2H-CC and 3H-CC. Below this interval, preservation of calcareous nannofossils is poor as a result of overgrowth. The top of *Pseudoemiliania lacunosa* in Sample 166-1004A-5H-CC defines the base of NN20 (0.41 Ma). *P. lacunosa*, *Gephyrocapsa caribbeanica*, and *Gephyrocapsa oceanica* are present in Samples 166-1004A-5H-CC through 18X-CC and are correlated to Zone NN19. In this interval, the first occurrence of *Gephyrocapsa parallela* (just above the Jaramillo Event; 0.95 Ma) was detected between Samples 166-1004A-9H-CC and 10H-CC. The concurrent range of *G. parallela* and *Reticulofenestra asanoi* is between 0.95 and 0.85 Ma. Because *R. asanoi* was not found in these samples, this level must be younger than 0.85 Ma.

The Pliocene/Pleistocene boundary is placed between Samples 166-1004A-18X-CC and 19X-CC on the basis of the first occurrence of *G. caribbeanica*, which is traceable to just above the Pliocene/Pleistocene boundary at its stratotype in Italy. Samples 166-1004A-

19X-CC and 22X-CC are characterized by the presence of *P. lacunosa* and the absence of discoasters. In Holes 1003A and 1003B, a similar floral assemblage is present in Samples 166-1003A-14X-CC through 18X-CC and 166-1003B-13X-CC through 17X-CC, which are between the base of *G. caribbeanica* (1.72 Ma) to the top of *Discoaster tamalis* (2.75 Ma). Therefore, Samples 166-1004A-19X-CC and 22X-CC probably correlate to the upper Pliocene Zones NN16–18.

### Planktonic Foraminifers

Planktonic foraminifers recovered from Hole 1004A are generally poorly preserved in the samples examined except in the uppermost Pleistocene sediments. Below this level, planktonic foraminiferal abundance varies considerably from barren to abundant, whereas preservation is only poor to moderate. Reworking of a few older Miocene specimens was noted in several samples. Planktonic foraminiferal events are listed in Table 2 and shown in Figure 6.

It is not possible to place accurately the N22/21 zonal boundary (2.0 Ma) using planktonic foraminifers because of the poor preservation and low abundances in the lower Pleistocene and uppermost Pliocene sediments. The first occurrence of *Globorotalia truncatulinoides* marks this boundary and occurs in Sample 166-1004A-13X-CC. Calcareous nannofossils indicate that this level is in the “mid” Pleistocene, and that the N22/21 boundary should occur within or below Core 166-1004A-19X. Foraminifers are rare at best and poorly preserved in Cores 166-1004A-14X through 19X. Planktonic foraminifers in Sample 166-1004A-22X-CC include *Globorotalia limbata* and *Globorotalia pertenuis*, placing this level in the upper Pliocene Zone N21.

### Benthic Foraminifers

The Pleistocene section at Hole 1004A yields well-preserved benthic foraminiferal faunas that contain *Bulimina marginata* (~30–600 m), *Cibicidoides cicatricosus* (>200 m), *Cibicidoides mundulus* (>200 m), *Cibicidoides incrassatus* (~100–600 m), *Planulina foveolata* (~100–500 m), *Planulina ariminsensis* (~100–800 m), and *Sigmilopsis schlumbergeri* (>200 m) (van Morkhoven et al., 1986), indicating a paleodepth of ~200–500 m (within the upper bathyal zone). Other common taxa typical of the upper bathyal assemblages

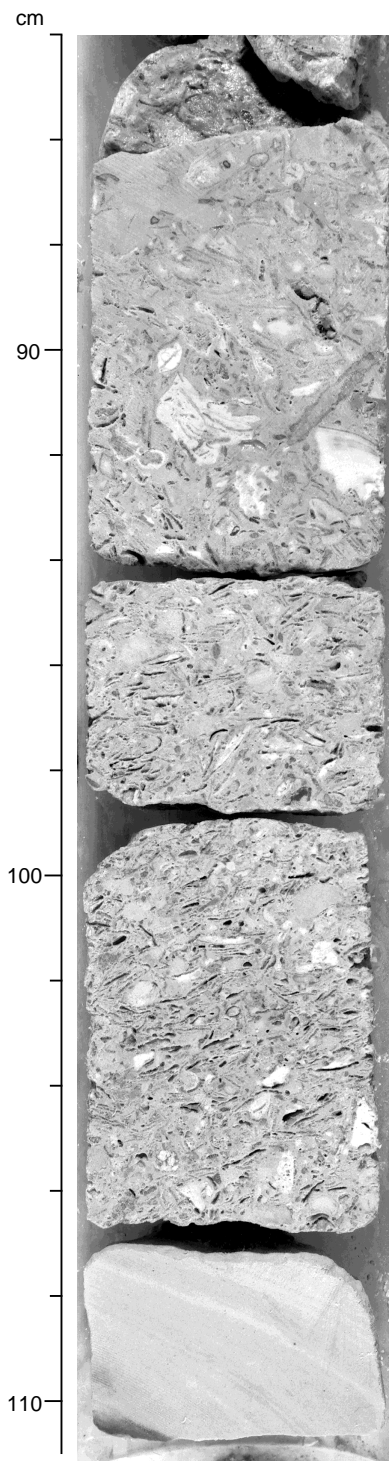


Figure 5. Close-up photograph of the bottom part (84–111 cm) of the bioclastic floatstone occurring in interval 166-1004A-16X-1, 67–112 cm. This floatstone consists of *Halimeda* fragments, coral debris, red algae, bivalves, benthic foraminifers, and lithoclasts. Some of the skeletal grains are blackened. The interval has significant moldic porosity with bladed to prismatic cements infilling dissolution voids.

in this section are similar to those found at Site 1003 (see “Biostratigraphy” section, “Site 1003” chapter, this volume).

The Pleistocene section also contains diverse, platform-derived shallow-water taxa that are similar to those found at Site 1003 (see “Biostratigraphy” section, “Site 1003” chapter, this volume); however, the platform-derived faunas are slightly more diverse and abundant at Site 1004 than they are at coeval levels at Site 1003. The diversity and abundance of the transported taxa drop significantly between Cores 166-1004A-9H and 10H, as do the preservation and diversity of the in situ faunas.

Upper Pliocene Samples 166-1004A-19X-CC and 22X-CC contain upper bathyal faunas with poor to moderate preservation. These samples contained no platform-derived species nor did they contain the reworked deep-water Eocene species that were found at coeval levels at the deeper water Site 1003, indicating that the mechanism responsible for deposition of the transported older taxa at Site 1003 did not extend to the shallower Site 1004.

### Sedimentation Rates

Sediments at Site 1004 yielded several nannofossil datum levels and two planktonic foraminiferal biohorizons. Age vs. depth is plotted on Figure 6. The sedimentation rate was high throughout the Pleistocene (9 cm/k.y.). Modern platform production and shedding on its leeward side began to affect this location at about 1.7 Ma (~Pliocene/Pleistocene boundary), much earlier than the more distal Site 1003, which shows an increase in sedimentation at about 1 Ma (see “Biostratigraphy” section, “Site 1003” chapter, this volume).

Age control for the upper Pliocene section is restricted to Sample 166-1004A-22X-CC, which contains the planktonic foraminifer *G. pertenuis*, indicating an age older than 2.6 Ma, whereas the nannofossil *D. tamalis* is absent, indicating an age younger than 2.75 Ma. This age constraint yields a late Pliocene sedimentation rate of approximately 3 cm/k.y. at Site 1004, similar to the late Pliocene sedimentation rate at Site 1003, indicating normal pelagic sedimentation at both sites during this period.

### PALEOMAGNETISM

Shipboard paleomagnetic measurements were conducted at Hole 1004A on the archive-half of cores at 20-cm intervals. Measurements, using a whole-core cryogenic magnetometer with in-line AF demagnetizer, were made of the natural remanent magnetization (NRM) and the response of the sediment cores to demagnetization steps of 0 and 10 or 15 mT. NRM values ranged from 87 to 0.2 mA/m, with typical intensities between 4.00 and 0.40 mA/m (Fig. 7). The NRM record shows a series of fluctuations that also can be seen in the magnetic susceptibility record (see below) and may represent intervals during which magnetic mineral preservation varied. After demagnetization at 15 or 10 mT, the NRM was characteristically reduced by less than 50% and varied from 2.90 to 0.14 mA/m, with an average value of 0.80 mA/m. Saturation isothermal remanent magnetization (SIRM) acquisition tests were conducted on individual samples from the working-half of Cores 166-1004A-1H through 11H (i.e., 1H-1, 91–93 cm; 2H-5, 135–136 cm; 3H-3, 118–120 cm; 4H-2, 104–106 cm; 5H-1, 61–63 cm; 6H-1, 95–97 cm; 7H-1, 125–127 cm; 9H-1, 135–137 cm; 9H-2, 9–11 cm; 10H-3, 12–14 cm; and 11H-1, 10–12 cm) and suggest that, throughout Hole 1004A, the remanence is carried by single-domain titanomagnetite (Fig. 8) with little variation in grain size or composition.

The magnetic susceptibility record for Hole 1004A was generated by whole-core MST measurements (Fig. 7B, corrected for spikes at core boundaries). The susceptibility signal was dominated by a diamagnetic response (negative), typical for carbonate sediments, with two positive susceptibility spikes at 78.05–79.65 mbsf (Sections 166-1004A-10H-2 to 10H-3) and 107.95–113.05 mbsf (Sections 166-

**Table 2. Calcareous nannofossil and planktonic foraminiferal bioevents.**

Event	Age (Ma)	Interval (cm)	Depth (mbsf)
<b>Calcareous nannofossils</b>			
B <i>E. huxleyi</i> (NN20/21)	0.25	1004A-2H-CC to 1004A-3H-CC	19.43
T <i>P. lacunosa</i> (NN19/20)	0.41	1004A-4H-CC to 1004A-5H-CC	38.56
T <i>R. asanoi</i>	0.85	1004A-9H-CC to 1004A-10H-CC	81.16
B <i>G. caribbeanica</i> (NN18/19)	1.72	1004A-18X-CC to 1004A-19X-CC	152.03
T <i>D. tamalis</i>	2.75	>1004A-22X-CC	186.43
<b>Planktonic foraminifers</b>			
T <i>G. obliquus</i>	1.3	1004A-13X-CC to 1004A-14X-CC	109.06
T <i>G. pertenuis</i>	2.6	1004A-22X-CC	186.43

Note: B = base, T = top.

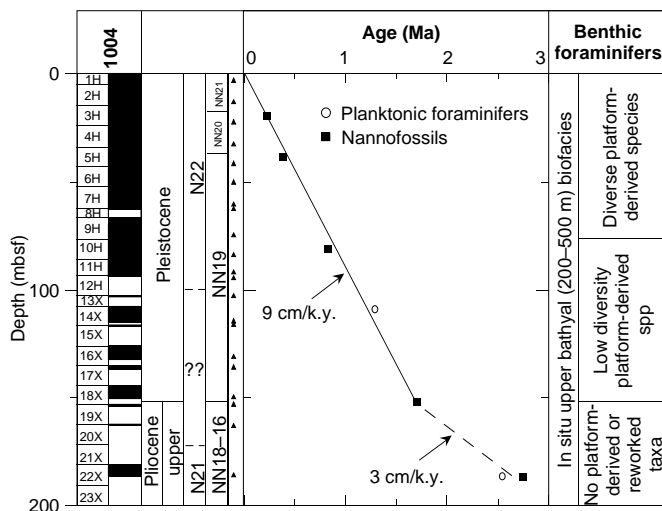


Figure 6. Calcareous nannofossil and planktonic foraminiferal zonation and benthic foraminiferal faunal changes for Site 1004. Recovery for each hole is adjacent to the cores. Solid triangles mark the position of samples examined for stratigraphy and benthic foraminiferal faunas. The age-depth plot is based on the biohorizons in Table 2.

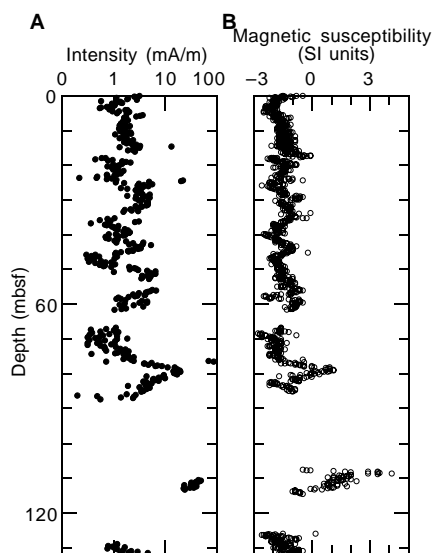


Figure 7. Archive-half NRM intensity (A) and whole-core magnetic susceptibility (B) profile for the interval from 0 to 132 mbsf in Hole 1004A.

1004A-14X-1 to 14X-4). Magnetic susceptibility fluctuations correlate well with variations in NRM intensity (Fig. 7); low NRM intensity correlating with more strongly diamagnetic behavior. The uniform magnetic mineralogy of Hole 1004A suggests that variations in diamagnetic behavior may reflect differences in magnetic mineral content. Downhole NRM and magnetic susceptibility data correlate closely with the spectrophotometer-reflected light scans of Hole 1004A (see Fig. 4, "Lithostratigraphy" section, this chapter). Darker intervals of sediment, possibly representing periods of reduction, appear to correlate well with lows in NRM intensity and magnetic susceptibility. This suggests that fluctuations in the diamagnetic susceptibility signal may reflect varying degrees of dilution of ferrimagnetic and antiferrimagnetic grains by carbonate during periods of poor magnetic grain preservation.

Variations in magnetic inclination downhole (Fig. 9), before and after demagnetization, were used to define a tentative series of polarity zones. Inclination values before demagnetization ranged from  $83^\circ$  to  $-78^\circ$ , with an average value of  $54^\circ$ . Only 1% of the NRM values possessed negative inclinations, indicating a dominantly normal polarity NRM component. Demagnetization at 10 or 15 mT caused a reduction in inclination of approximately  $29^\circ$ , with an increase of negatively inclined measurement intervals (3%). Between 0 and 71.15 mbsf, an average inclination of  $31^\circ$  is observed, suggesting an interval of normal polarity. Eighty-six percent of the negatively inclined measurement intervals were located between 71.15 and 78.85 mbsf, suggesting an interval of reverse polarity. From 78.85 to 86.25 mbsf, the inclination is positive with an average value of  $28^\circ$ . This may represent an interval of normal polarity.

Two tentative reversal boundaries can be correlated. The predominantly normal polarity between 0 and 71.15 mbsf is correlated with the Brunhes Chron, with an age less than 0.78 Ma. The Brunhes/Matuyama boundary is placed provisionally at 71.15 mbsf (Section 166-1004A-9H-5, 25 cm). This correlation is based on the first occurrence of the nannofossil *Gephyrocapsa parallela*, which appears just above the Jaramillo Event (0.95 Ma) and between Samples 166-1004A-9H-CC and 10H-CC. The upper boundary of the normal polarity Jaramillo Event is provisionally placed at 78.85 mbsf (Section 166-1004A-10H-2, 105–145 cm).

## ORGANIC GEOCHEMISTRY

At Site 1004, the shipboard organic geochemistry program included determinations of inorganic carbon, total carbon, total nitrogen, total sulfur, and Rock-Eval pyrolysis, in addition to safety monitoring for hydrocarbon gases. The analytical procedures are described in the "Explanatory Notes" chapter (this volume).

### Volatile Hydrocarbons and Hydrogen Sulfide

At Site 1004, the methane ( $C_1$ ) concentration in the headspace gases is low (2–4 ppm) in the upper 40 m. Between 49.3 and 74.3

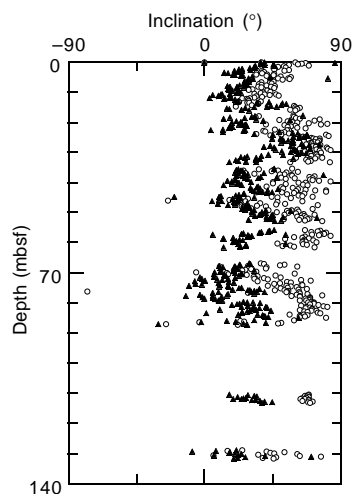


Figure 8. NRM (open circles) and 10- or 15-mT demagnetization step (solid triangles) inclination variation for Hole 1004A between 0 and 132 mbsf.

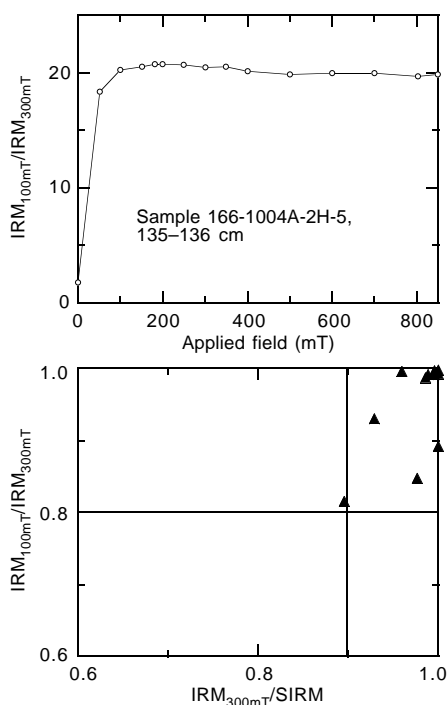


Figure 9. Isothermal remanent magnetization acquisition curve for Sample 166-1004A-2H-5, 135–136 cm (periplatform carbonate ooze), and a plot of  $IRM_{300mT}/SIRM$  vs.  $IRM_{100mT}/IRM_{300mT}$  for samples taken from the working half of Cores 166-1004A-1H through 11H. All the data are closely grouped within the single-domain magnetite region of the plot, suggesting that little variation is present in either grain size or composition.

mbsf, methane shows a steady increase from 17 to 6692 ppm (Table 3 on CD-ROM; Fig. 10). High methane concentrations (>10,000 ppm) were observed below 83.3 mbsf. Ethane ( $C_2$ ) was detected at 49.3 mbsf (Table 3 on CD-ROM). The  $C_1/C_2$  ratio below 62.2 mbsf ranges from 1673 to 3391 with no systematic variation (Fig. 10).

Propane ( $C_3$ ) was first observed at 74.3 mbsf; below 91.8 mbsf, trace levels (0.2–4 ppm) of isobutane, *n*-butane, isopentane, and *n*-pentane also were found (Table 3 on CD-ROM). The concentration

of hydrogen sulfide ( $H_2S$ ) increased between 62.0 mbsf (368 ppm) and 83.8 mbsf (21,150 ppm). At greater depths, the  $H_2S$  concentration decreased slightly (Fig. 10).

### Inorganic and Total Organic Carbon, Total Sulfur, and Total Nitrogen

Carbonate data for Site 1004 are presented in Figure 11 and in Table 4 on CD-ROM. The total carbonate concentration varies from 91 to 96 wt% (Fig. 11). Seven samples at Site 1004 with low carbonate content were selected for total carbon, total sulfur, and total nitrogen analysis. Total organic carbon (TOC) at Site 1004 varies from 0.49 to 2.62 wt% (Fig. 11). High concentrations (>1.0 wt%) are observed in lithologic Subunit IB at 78.19, 91.3, and 112.4 mbsf. Total sulfur (TS) concentrations at Site 1004 are low (0.07–0.26 wt%) (Table 4 on CD-ROM). Total nitrogen (TN) ranges from 0.04 to 0.11 wt% (Table 4 on CD-ROM).

### Characterization and Maturity of Organic Matter

Seven samples with TOC greater than 0.5 wt% were characterized by Rock-Eval pyrolysis. The results are reported in Table 5 on CD-ROM and in Figure 11.  $T_{max}$  ranges from 421° to 435°C at Site 1004. The highest  $T_{max}$  values (>430°C) are observed in the topmost part of the section (38.7 and 57.7 mbsf). The hydrogen index (HI) varies from 240 to 551 mg HC/g TOC.

### Discussion

The high  $C_1/C_2$  ratio (>1000) observed below 74.3 mbsf at Site 1004 indicates that a significant amount of biogenic methane is produced in the sediment. The low  $C_1/C_2$  ratio in the upper part (above 62.3 mbsf) of the section is probably a result of preferential loss of  $C_1$  by either diffusion or selective microbiological  $C_1$  consumption (Claypool and Kvenvolden, 1983). The range in  $T_{max}$  at Site 1004 indicates that the organic matter is immature with regard to oil formation. The two samples with  $T_{max}$  greater than 430°C (at 38.7 and 57.7 mbsf) are not thought to reflect thermal maturity. These high  $T_{max}$  values probably are caused by preferential oxidation of the organic matter.

The high  $H_2S$  concentrations observed below 60.3 mbsf coincide with a reduction in interstitial  $SO_4^{2-}$  concentrations, indicating the oxidation of organic matter by sulfate-reducing bacteria. However, the presence of trace levels of higher weight hydrocarbons in the head-space gases below 74.3 mbsf indicates that nonbiological decomposition of organic matter also contributes to some of the gas composition at Site 1004.

High TOC contents (>1 wt%) are observed in intervals dominated by calcareous nannofossils and peloids (see "Lithostratigraphy" section, this chapter). The organic matter in these intervals is characterized by high HI values (436–551 mg HC/g TOC), which indicate a marine origin. Samples with low TOC content (<1 wt%) are characterized by lower HI (240–300 mg HC/g TOC), which suggests either a mixed marine and terrestrial environment or an oxidized marine origin for the organic matter.

## INORGANIC GEOCHEMISTRY

Inorganic chemical analyses were conducted on 20 interstitial water samples squeezed from whole-round samples at a frequency of one per every other section in the first three cores and one per core thereafter. Analytical methods are detailed in the "Inorganic Geochemistry" section of the "Explanatory Notes" chapter (this volume). The concentrations of dissolved interstitial constituents measured at Site 1004 are shown in Table 6, and the profiles are shown

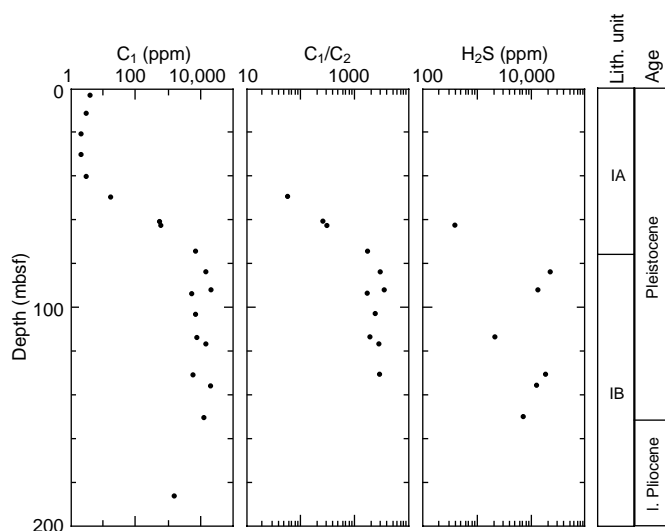


Figure 10. Methane concentrations ( $C_1$ ), methane/ethane ( $C_1/C_2$ ) ratios, and (C) hydrogen sulfide ( $H_2S$ ) of headspace gases from Site 1004. Subunits IA and IB are lithologic subunits (see “Lithostratigraphy” section, this chapter).

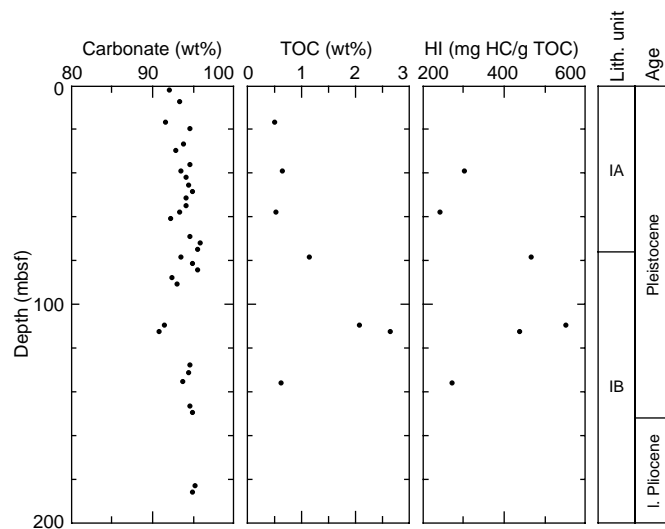


Figure 11. Concentration of carbonate, total organic carbon, and hydrogen index (HI) at Site 1004. Subunits IA and IB are lithologic subunits (see “Lithostratigraphy” section, this chapter).

in Figure 12. To remove changes caused by large salinity variations, concentrations of selected ions were normalized to  $Cl^-$  (Fig. 13). Normalization of interstitial water ( $N$ )<sub>IW</sub> was achieved using the ion ratio from surface seawater collected at Site 1003 and is expressed as deviations (mM and  $\mu$ M) by the expression

$$(N)_{IW} = (x_{IW}) - x_{sw} \left( \frac{Cl_{IW}}{Cl_{sw}} \right) \quad (1)$$

The mineralogy of the carbonate portion of the sediments at Site 1004 was quantified by X-ray diffraction (XRD) at a frequency of one per section (Fig. 14). Ninety samples were analyzed. All carbonate mineralogy data were corrected to include the noncarbonate fraction as determined by total carbonate analysis (see “Organic Chemistry” section, this chapter) and are presented in Table 7 on CD-ROM.

## Interstitial Waters

### Salinity, Chloride, Sodium, and Potassium

Salinity and chloride ( $Cl^-$ ) profiles measured at Site 1004 show little change in the upper part of the section (0 to 40 mbsf). Below this zone, there is a sharp and continuous rise in  $Cl^-$  to a value of 759 mM at the bottom of the hole (approximately 200 mbsf). In the upper 40 mbsf, the lack of a measurable  $Cl^-$  gradient indicates that seawater is probably being flushed through this shallow zone at sufficiently high rates to remove diffusional gradients. Lithified layers in these shallow sediments probably act as relatively impermeable barriers between the lower salinity formation water and normal seawater (see “Lithostratigraphy” section, this chapter).

The sodium ( $Na^+$ ) concentrations remain conservative with respect to  $Cl^-$  over the entire core length, showing no change with depth from normal seawater ratios within the analytical precision (see “Explanatory Notes” chapter, this volume). Normalized potassium ( $K^+$ ) concentrations show a small increase with depth, reaching a maximum enrichment of 1.5 mM near the base of the hole (Fig. 13). This increase corresponds well to the measured increase in ammonium ( $NH_4^+$ ) and has been postulated to be caused by ion-exchange reactions involving organic-rich layers (Gieskes, 1983; Mackin and Aller, 1984).

### Alkalinity, Sulfate, Ammonium, and Phosphate

The titration alkalinity and sulfate ( $SO_4^{2-}$ ) concentrations at Site 1004 both show major changes below the boundary at 40 mbsf. The alkalinity increases significantly from seawater concentrations (2.5 mM) to a maximum concentration of 73.5 mM at a depth of 93 mbsf and remains near this level to the base of the hole. Over the same interval,  $SO_4^{2-}$  mirrors the alkalinity profile at close to the expected 2:1 ratio. Sulfate is completely exhausted by a depth of 75 mbsf. Complete  $SO_4^{2-}$  removal is defined here to be within the  $SO_4^{2-}$  contamination limits of 0–2 mM caused by drilling fluids. Steep increases in methane concentrations at the base of the sulfate-reduction zone (75 mbsf) indicate that active methanogenesis is occurring below 75 mbsf (see “Organic Geochemistry” section, this chapter).

Organic remineralization processes are also reflected in the  $NH_4^+$  profile, which increases rapidly in the sulfate-reduction zone to 15 mM and then shows a more gradual increase to the base of the hole, where it reaches a concentration of 19 mM. The occurrence of the  $NH_4^+$  peak at greater depths than the alkalinity peak is probably caused by differences in microbial end-products within the sulfate-reduction zone and lower methanogenic zone. The asymptotic increase in  $NH_4^+$  below 90 mbsf probably reflects a gradual decline in the concentration of organic matter in deeper parts of the core.

Phosphate ( $HPO_4^{2-}$ ) concentrations range from 1 to 10  $\mu$ M, showing a much smaller increase and more variable distribution than expected based on the marine Redfield N:P ratio of 16:1. Calculated N:P ratios for Site 1004 pore waters are in excess of 1000:1, and suggest active removal of  $HPO_4^{2-}$  from pore waters. Two likely sinks are (1) precipitation of carbonate fluorapatite (CFA) (Gaudett and Lyons, 1980), and (2) adsorption of reactive phosphate onto carbonate grains (Kitano et al., 1978). Preliminary calculations of saturation states using measured fluoride ( $F^-$ ) concentrations suggest that pore waters are supersaturated with respect to apatite and probably CFA as well. In addition, the presence of blackened, possibly phosphatized, grains within lithologic Subunit IA (see “Lithostratigraphy” section, this chapter) indicate that these sediments are an important sink for  $HPO_4^{2-}$ .

### Calcium, Magnesium, Strontium, and Lithium

Calcium ( $Ca^{2+}$ ) and magnesium ( $Mg^{2+}$ ) both show sharp decreases downhole below 40 mbsf from seawater concentrations (10.9 and 57

Table 6. Composition of interstitial waters from Site 1004.

Core, section, interval (cm)	Depth (mbsf)	pmH	pH	Alk (mM)	Sal	Cl <sup>-</sup> (mM)	Na <sup>+</sup> (mM)	Mg <sup>2+</sup> (mM)	Ca <sup>2+</sup> (mM)	SO <sub>4</sub> <sup>2-</sup> (mM)
166-1004A-										
1H-1, 145-150	1.5		7.59	2.73	36.5	560	490	56.0	11.2	29.8
1H-3, 145-150	4.5		7.67	2.71	36.5	571	496	56.5	11.4	29.5
2H-1, 140-150	6.7		7.80	2.84	36.5	575	499	56.2	11.6	30.2
2H-3, 140-150	9.7		7.75		36.5	576	499	56.2	11.5	29.1
2H-5, 140-150	12.7		7.74	3.25	36.5	575	496	56.3	11.2	29.7
3H-1, 140-150	16.2		7.66	2.62	36.5	575	492	56.1	11.1	29.3
3H-3, 140-150	19.2		7.57	2.43	36.5	574				29.8
3H-5, 140-150	19.2		7.62	2.46	36.5	562	498	55.3	10.7	29.3
4H-4, 140-150	30.2		7.64	2.49	36.5	575	498	55.9	11.0	28.9
5H-5, 140-150	41.2	7.61	7.52	3.22	36.5	571	498	56.1	11.5	29.2
6H-5, 140-150	50.7	7.02	7.57	14.37	37.0	579	504	54.5	12.2	25.4
7H-5, 140-150	60.2	6.58	7.64	37.72	39.0	615	530	50.9	9.0	13.1
9H-5, 140-150	74.2	6.58	7.46	64.80	42.0	662	577	45.4	6.4	2.6
10H-5, 140-150	83.7	6.58	7.24	69.99	43.0	685	599	43.0	6.0	2.2
11H-5, 92-102	92.7	6.56	7.24	73.41	44.0	680	605	43.1	6.7	1.2
14X-2, 140-150	110.4	6.63	8.03	69.41	45.5	711	628	40.8	6.9	3.2
16X-3, 135-150	130.4	6.58	7.98	65.23	46.0	728	640	38.8	6.1	2.3
18X-4, 89-105	149.8	6.58	6.78	65.20	46.0	734	642	39.0	6.1	2.1
22X-3, 135-150	185.6	6.54	7.92	68.32	46.5	759	652	37.7	6.4	0.3

Table 6 continued.

Core, section, interval (cm)	Depth (mbsf)	HPO <sub>4</sub> <sup>2-</sup> (μM)	NH <sub>4</sub> <sup>+</sup> (μM)	H <sub>4</sub> SiO <sub>4</sub> (μM)	K <sup>+</sup> (μM)	Li <sup>+</sup> (μM)	Sr <sup>2+</sup> (μM)	F <sup>-</sup> (μM)	Fe <sup>2+</sup> (μM)
166-1004A-									
1H-1, 145-150	1.5	0.6	61	41	10.3	28	100		6.4
1H-3, 145-150	4.5	0.7	63	24	10.5	28	101	84	4.2
2H-1, 140-150	6.7	1.0	108	28	10.5	27	96	75	6.5
2H-3, 140-150	9.7	1.0	152	37	10.3	28	98	76	5.0
2H-5, 140-150	12.7	2.1	149	49	10.2	29	101	76	4.4
3H-1, 140-150	16.2	1.5	85	41	10.4	30	102	75	3.4
3H-3, 140-150	19.2	0.9	41	24		29	101	74	2.2
3H-5, 140-150	19.2	0.9	54	24	10.5	29	103	77	5.1
4H-4, 140-150	30.2	0.9	115	20	10.3	29	115	79	5.8
5H-5, 140-150	41.2	1.5	1,687	28	10.6	30	138	90	2.8
6H-5, 140-150	50.7	3.6	1,617	58	10.7	37	262	112	0.5
7H-5, 140-150	60.2	4.9	5,131	193	11.6	64	734	196	1.9
9H-5, 140-150	74.2	6.2	8,300	420	12.3	90	1,070	296	0.0
10H-5, 140-150	83.7	4.7	11,867	497	12.8	102	1,190	326	0.0
11H-5, 92-102	92.7	4.6	13,781	507	13.3	106	1,365	328	0.0
14X-2, 140-150	110.4	9.0	14,912	864	13.7	113	1,442	389	0.0
16X-3, 135-150	130.4	4.1	16,275	734	14.2	116	1,567	403	0.0
18X-4, 89-105	149.8	4.3	16,478	444	14.5	118	1,647	445	1.8
22X-3, 135-150	185.6	4.1	19,117	551	15.2	147	2,530	357	1.1

mM, respectively) to normalized losses of 8 and 27 mM, respectively (Fig. 13). These changes are interpreted to be caused by carbonate dissolution and precipitation reactions. Within the sulfate-reduction zone, the low amounts of SO<sub>4</sub><sup>2-</sup>, high alkalinity, and active microbial activity may provide a favorable geochemical environment for dolomite formation (Baker and Kastner, 1981; Kastner et al., 1990). Dolomitization by a combination of the reactions listed below is proposed to explain the progressive loss of Ca<sup>2+</sup> and Mg<sup>2+</sup> in Hole 1004A.



The first reaction results in a 1:1 decrease in Ca<sup>2+</sup>:Mg<sup>2+</sup>, whereas the second reaction results in a 0:1 decrease. At Site 1004, the ratio of Ca<sup>2+</sup>:Mg<sup>2+</sup> lost is on the order of 1:3, suggesting that replacement dolomitization by the second reaction may be the dominant carbonate reaction.

The concentration of dissolved strontium (Sr<sup>2+</sup>) increases significantly below 40 mbsf from seawater concentrations (94 μM) to a high of 2.5 mM at the bottom of the hole. The Sr<sup>2+</sup> is supplied to pore fluids by the dissolution and recrystallization of aragonite to diagenetic high- and low-Mg calcite and dolomite. The maximum amount of

Sr<sup>2+</sup> that can accumulate in these SO<sub>4</sub><sup>2-</sup>-depleted zones will depend on the amount of aragonite dissolution, the rate of pore-water movement, and the solubility of celestite (SrSO<sub>4</sub>). Dissolved lithium (Li<sup>+</sup>) concentrations generally follow the Sr<sup>2+</sup> profiles as seen at Site 1003, suggesting that Li<sup>+</sup> may be involved in carbonate recrystallization reactions (see "Inorganic Chemistry" section, "Site 1003" chapter, this volume, for a more detailed discussion).

#### Silica, Fluoride, pmH, and Iron

Silica (H<sub>4</sub>SiO<sub>4</sub>) concentrations increase abruptly below 40 mbsf to a maximum of 800 μM at 110 mbsf. Fluoride concentration also increases sharply to a maximum value of 445 μM at a depth of 150 mbsf. The depth of maximum dissolved F<sup>-</sup> corresponds to the Pliocene/Pleistocene boundary. This increase is similar to Site 1003. A possible explanation for the peak in F<sup>-</sup> at this boundary is that it reflects the presence of CFA in the sediments. The pmH remains above 7.4 down to a depth of 40 mbsf, below which it declines sharply through the sulfate-reduction zone to values near 6.5. Below this depth, pmH remains constant to the base of the hole. Iron (Fe<sup>2+</sup>) concentrations (not shown) are highest at the top of the hole (4–7 μM), dropping to less than the detection limit (2 μM) in the deeper samples.

#### Mineralogy

The mineralogy of Site 1004 is dominated by a mixture of stable carbonates (low-magnesium calcite [LMC] and dolomite) and meta-

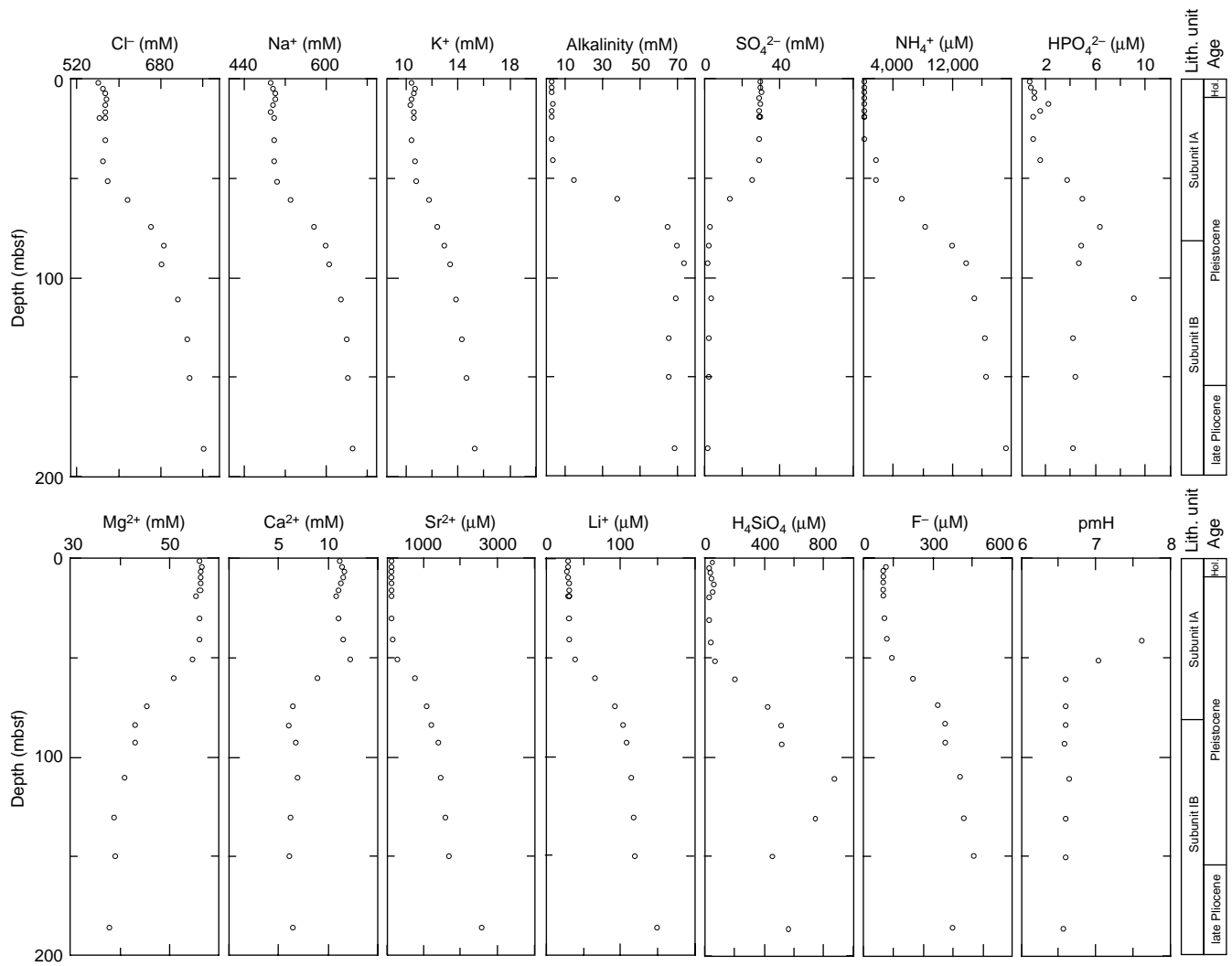


Figure 12. Depth profiles of interstitial water constituents at Site 1004.

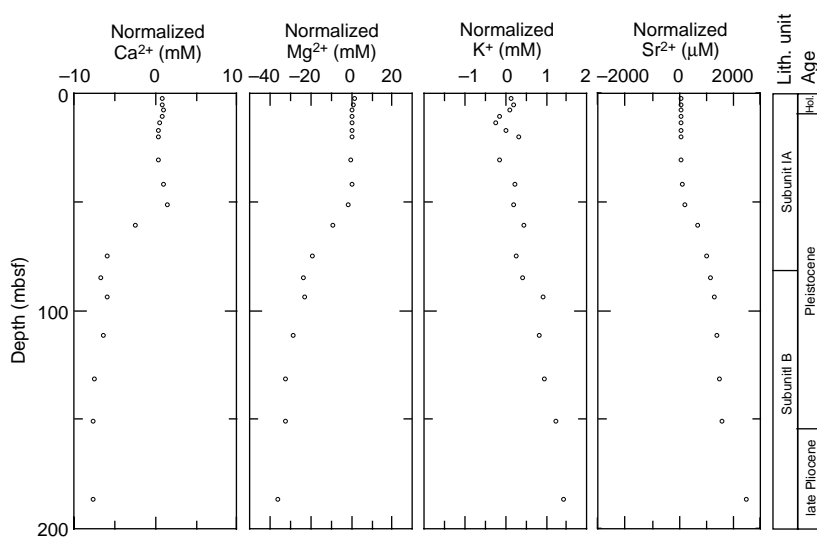


Figure 13. Seawater-normalized depth profiles of selected interstitial water constituents at Site 1004.

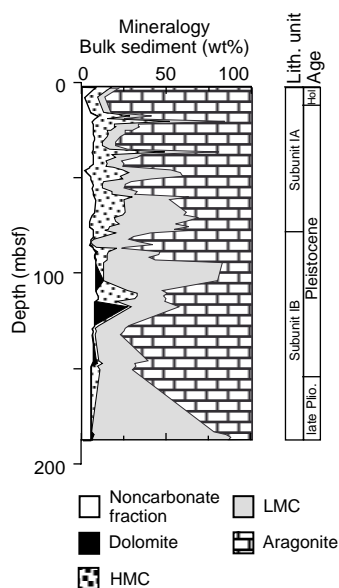


Figure 14. Quantitative X-ray mineralogy of sediments from Site 1004.

stable carbonates (aragonite and high-magnesium calcite [HMC]). Carbonates make up 91 to 97 wt% of the bulk sediments, and the remainder of the sediment consists of organic carbon, biogenic silica, and clays (see “Organic Geochemistry” section, this chapter). Perhaps the most striking feature in the core is the change in abundance of aragonite in the upper 100 m. These changes in aragonite occur in distinct cycles thought to correspond to high-frequency glacial sea-level changes throughout the Pleistocene (see “Lithostratigraphy” section, this chapter). The abundance of HMC and LMC increases noticeably at the aragonite minimums, probably reflecting the increased role of marine seafloor cementation during lowstand sea-level events (Schlager and James, 1978).

Dolomite first occurs at a depth of 85 mbsf, corresponding to a pronounced minimum in the HMC abundance in the uppermost portion of Subunit IB. The occurrence of dolomite spikes (up to 22%) at depths of 100, 110, and 145 mbsf is probably a consequence of the localized dolomite distribution in these sediments and of poor recovery in this lower portion of the core. Presumably, the dolomite below 100 mbsf is restricted to horizontal layers, similar to the shallow hardground layers found in the shallower portions of the core.

## PHYSICAL PROPERTIES

Physical properties measurements at Hole 1004A were conducted using the methods described in the “Physical Properties” section of the “Explanatory Notes” chapter (this volume). Measurements were made both on whole cores, using the MST, and from discrete positions on the split cores. MST measurements were made every 15 cm for NGR and every 5 cm for magnetic susceptibility, GRAPE density, and velocity. Velocity measurements on the MST were not taken in cores that were indurated, as gaps between the core and liner prevent the transmission of the acoustic signal. On all cores, three discrete velocity measurements were taken per section, one of which was measured for index properties. Differences seen between GRAPE bulk density and bulk density measured on discrete samples were partially corrected for, as explained in the “Physical Properties” section in the “Explanatory Notes” chapter.

The following sections discuss the downhole variations in petrophysical properties and their correlation to the lithostratigraphy.

Magnetic susceptibility data are discussed within the “Paleomagnetism” section (this chapter).

## Index Properties, GRAPE Density, and *P*-Wave Velocity

Tables 8 through 15 on CD-ROM list all the physical properties data collected at this site. In general, the data at Site 1004 show patterns similar to those seen in the upper intervals at Site 1003. The data at Site 1004 can be divided into zones with distinct petrophysical signatures that show fundamental changes in character for the different data sets measured (Figs. 15, 16).

Petrophysical Unit I (0–18 mbsf) consists of an interval that has a lower variability in petrophysical properties than in the unit below. This unit correlates well with petrophysical Subunit IA from Site 1003. Within Unit I, there is a downcore increase in *P*-wave velocities from 1.55 to 1.62 km/s near 4 mbsf that correlates with an increase in bulk density from 1.85 to 2.0 g/cm<sup>3</sup>, a decrease in magnetic susceptibility from –1.9 to –2.2 SI-units, and a decrease in porosity from 65% to 60% (Fig. 15). The increase in velocity was apparently not recorded as a lithologic change in the sediments and may be due to increased compaction and cementation downcore.

The base of petrophysical Unit I is marked by a sharp increase in GRAPE density (1.85 to 2.35 g/cm<sup>3</sup>) downcore within Core 166-1004A-3H. The density increase from 1.8 to 2.3 g/cm<sup>3</sup> across this unit boundary at Site 1004 is greater than that at Site 1003. NGR shows a significant increase near this boundary (up to 25 cps), but this increase occurs nearly 2 m below the Unit I/II boundary. Occurring with the NGR shift is a downcore decrease in porosity (60% to 53%). At the top of petrophysical Unit II, maximum *V<sub>p</sub>* values increase abruptly to 1.6 km/s, whereas minimum *V<sub>p</sub>* values remain the same, resulting in a larger range of velocities below the boundary (Fig. 16). This increase coincides with a lithologic change to partially lithified sediments and may represent the Pleistocene/Holocene boundary. The Unit I/II boundary is also evident as a shift to higher color intensity.

Petrophysical Unit II (18–85 mbsf) is characterized by more variable and higher values for the properties measured. The variations display a distinct cyclicity in the magnetic susceptibility and NGR data within this unit (Fig. 16). These cycles correlate well with variations in lithology as indicated by color intensity (see “Lithostratigraphy” section, this chapter). In general, *P*-wave velocities increase downcore within Unit II from an average of 1.5 to 1.65 km/s (Fig. 16). Near 65 mbsf in petrophysical Unit II, there is an increase in velocity (1.55 to 1.65 km/s) that is reflected in the NGR and the magnetic susceptibility, but not in the bulk density.

The lower portion of petrophysical Unit II corresponds with a downcore increase in variation of the physical property parameters corresponding with a change in the sediment lithology from lithologic Subunit IA to Subunit IB. Recovery within the lower portion of Unit II was low, and the precise location of specific changes in physical property parameters was difficult to determine. A major feature of this unit is an increase in *P*-wave velocity from 1.8 to 6.5 km/s between 136 and 142 mbsf. This increase corresponds to a decrease in porosity from an average of 65% to 17% and an increase in density from 1.8 to 2.6 g/cm<sup>3</sup>. This change occurs just above the Pliocene/Pleistocene boundary.

## Shear Strength

Shear strength measurements were made to a depth of 95 mbsf, below which the sediments became too indurated. Values from shear strength measurements are shown in Table 14 on CD-ROM. Shear strength varies between 5 and 65 kPa and does not show a typical increase with depth as expected. Instead, there are two distinct layers of increased shear strength within Unit II (Fig. 17). The first is between 50 and 60 mbsf, where the shear strength increases from 5 to 45 kPa.

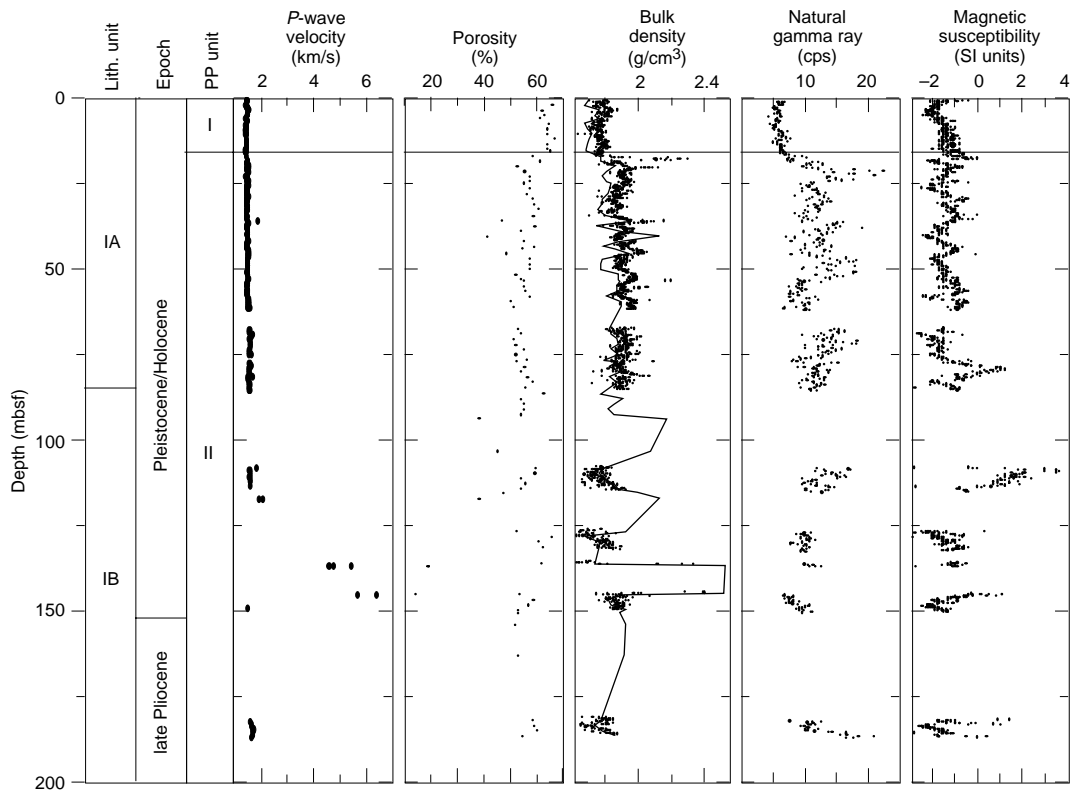


Figure 15. Combined plot of *P*-wave velocity from discrete measurements using the DSV and velocity frame, porosity, bulk density measured using the GRAPE (points) and discrete samples (line), NGR, and magnetic susceptibility from Hole 1004A. Lithologic and petrophysical units are indicated along with age. GRAPE density values were corrected for the mass-attenuation effect of water in high-porosity sediments (see “Explanatory Notes” chapter, this volume).

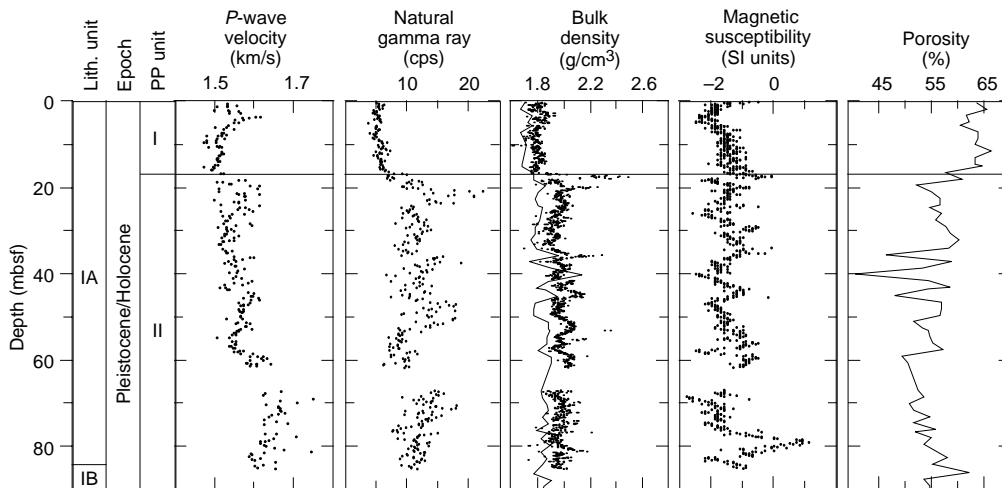


Figure 16. Summary of *P*-wave velocity from discrete measurements using the DSV and velocity frame, NGR, bulk density measured using the GRAPE (points) and discrete samples (line), magnetic susceptibility, and porosity for the interval from 0 to 90 mbsf. Lithologic and petrophysical units are indicated along with age. GRAPE density values were corrected for the mass-attenuation effect of water in high-porosity sediments.

The second interval (with values up to 65 kPa), occurs just above the lithologic Subunit IA/IB boundary. Unlike the shear strength variations at Site 1003, those at Site 1004 do not correspond with changes in the other petrophysical parameters measured. In addition, values are generally lower than at Site 1003; however, the  $S_v/P_o'$  ratio at Site 1004 shows a similar trend to that at Site 1003, with higher values at the surface and decreased values below (Fig. 17).

### Thermal Conductivity

A total of 62 thermal conductivity measurements were made from 0 to 200 mbsf on cores from Hole 1004A. Results are shown in Table 15 on CD-ROM and Figure 18. Thermal conductivity increases with depth from 0.95 to 1.2 W/(m·K) at 60 mbsf. The number of measurements made from 80 through 200 mbsf was limited because of poor

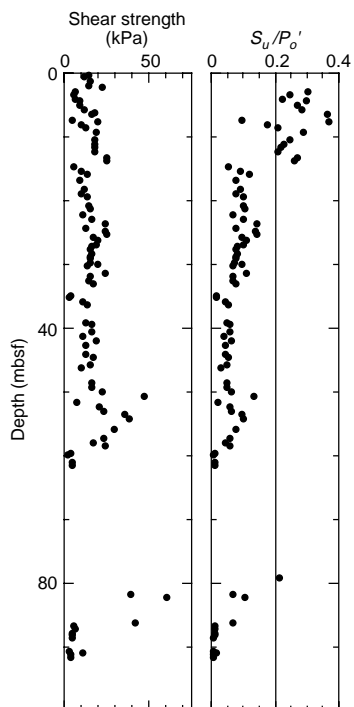


Figure 17. Shear strength and  $S_u/P_o'$  ratio calculated from shear strength and overburden stress for cores from Hole 1004A.

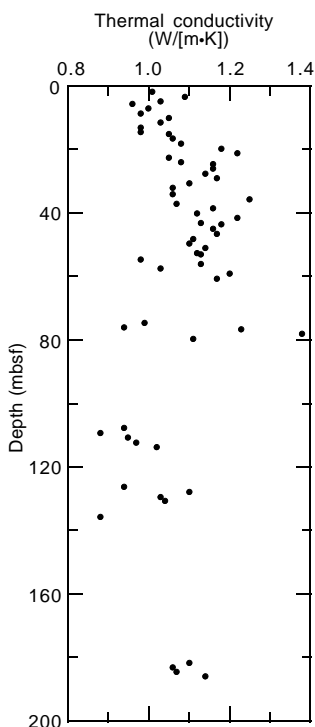


Figure 18. Thermal conductivity for Hole 1004A.

core recovery. The cores that were measured show conductivities lower than those measured between 40 and 60 mbsf. The average and the standard deviation of all the conductivity measurements at this site are 1.08 and 0.1 W/(m·K), respectively.

## IN SITU TEMPERATURE MEASUREMENTS

### Introduction

Ten in situ temperature measurements were made at Site 1004, using two sets of Adara tools and one unit of downhole water sampler, temperature, and pressure probes (WSTP). Six of the measurements were considered successful, and the remaining four were probably made in the bottom hole infill, which was cooled by drill water. The “In Situ Temperature Measurements” section of the “Explanatory Notes” and “Site 1003” chapters, this volume, explains the methods for determining the sediment equilibrium temperatures and the errors provided in Table 16. The temperature at the seafloor (~17.1°C) has been estimated from mudline stops.

### Geothermal Profile

Figure 19 shows the geothermal profile obtained from the measurements. The data from 62.3 through 181.2 mbsf show remarkable linearity. The linear regression coefficient for these points is 0.999. The two Adara measurement points at 33.8 and 43.3 mbsf fall on a smooth curve connecting this straight line and the mudline temperature point.

The shallow portion of the geothermal profile shows a concave upward feature. Typically such a profile suggests either a recent warming of the bottom water, a recent increase in sedimentation rate, or downward flow of the pore water. Sedimentation rates at this site almost doubled at about 2 Ma to 160 m/m.y. (see “Biostratigraphy” section, this chapter), but this alone would not affect the geothermal gradient much, and therefore, can be discounted. Some type of water circulation between the sediments and the bottom water is possible as salinity of the pore fluids of the cores shows no change from the seafloor down to about 50 mbsf (see “Inorganic Geochemistry” section, this chapter). There is no information available on the history of the bottom-water temperature of this area.

### Heat Flow

The lower straight part of the geothermal profile at Site 1004 gives a geothermal gradient of 35.7°C/km. The average of the thermal conductivities measured in the upper 200 mbsf is 1.08 W/(m·K), which yields a calculated heat flow value of 38.6 mW/m<sup>2</sup>. This agrees well with the first solution for the heat flow determination at Site 1003 (39.8 mW/m<sup>2</sup>).

## SEISMIC STRATIGRAPHY

Site 1004 penetrated the three Holocene–Pleistocene seismic sequences (*a*, *b*, and *c*) and reached the late Pliocene Sequence *d* (Figs. 20, 21). As a result of low recovery in the cores near the bottom of the hole, it is unclear whether seismic sequence Boundary D (SSB) was drilled or not. The correlation of these seismic sequences with lithologic and petrophysical parameters is discussed in the following paragraphs.

### Time-Depth Conversion

The measured velocities of the upper 200 mbsf at Site 1004 have similar overall values to those at Site 1003. We therefore used the time-depth curve of the VSP experiment at Site 1003 (see Fig. 42,

**Table 16. In situ bottom-hole sediment temperatures measured at Site 1004.**

Core	Depth (mbsf)	Temperature (°C)	Error (°C)	Mudline (°C)	Tool	Notes
166-1004A-						
4H	33.8	17.66	0.10	17.97	Adara11	
5H	43.3	17.85	0.18	17.09	Adara18	
7H	62.3	18.34	0.21	17.27	Adara11	
8H	71.8	17.60	0.22	16.98	Adara18	Anomalous, poor recovery
10H	90.8	19.35	0.02	17.39	Adara11	
12H	109.8	18.70	0.21	16.94	Adara18	Anomalous, poor recovery
17X	135.4	20.97	0.01	16.10	WSTP201	
20X	162.4	18.88	0.01	16.83	WSTP201	Anomalous, poor recovery
22X	181.2	22.57	0.01	17.45	WSTP201	
24X	200.0	20.69	0.01	17.03	WSTP201	Anomalous, poor recovery

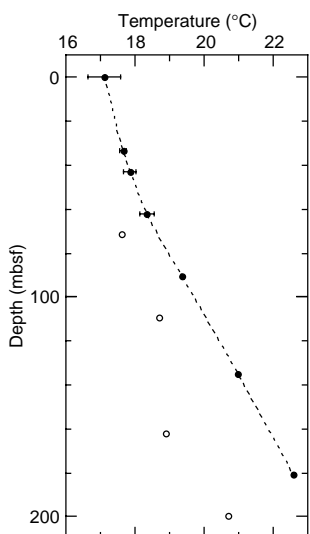


Figure 19. Geothermal profile at Site 1004. Solid circles represent the reliable temperature measurements, and open circles represent unreliable measurements.

“Site 1003” chapter, this volume) to correlate the seismic reflections to the Site 1004 cores.

### Holocene-Pleistocene Sequences

SSB A occurs on seismic Line 106a (Fig. 20) at 20 mbsf (TWT) or 20 mbsf (Table 17). SSB A is characterized in the shipboard velocity measurements by an abrupt increase in velocity and density and, consequently, an increase in acoustic impedance at the base of petrophysical Unit I (Fig. 20). In addition, it correlates with a strong positive gamma-ray excursion between 18 and 25 mbsf, with a maximum at 20 mbsf (Fig. 16). These increases in velocity, density, and gamma ray correlate with the first occurrence of submarine cementation and blackened grains and lithoclasts in the cores at 18 mbsf (see “Lithostratigraphy” section, this chapter), which may mark the Holocene/Pleistocene boundary. Above this coarse-grained layer, the sequence consists of unlithified mudstones to wackestones. On seismic Line 106a, Sequence *a* thins out basinward. In fact, at the more distal Site 1003, the equivalent first blackened horizon lies at a shallower depth, 12 mbsf, which shows good agreement between seismic geometry and the lithologic thickness.

SSB B was calculated to be at 70 mbsf (TWT) or 65 mbsf. This SSB corresponds to a subtle increase of velocities in the core at 60 mbsf (Fig. 20) and might coincide with a zone of three, closely spaced, cemented horizons between 45 and 67 mbsf, two of which contain lithoclasts with blackened grains that are intercalated within

peloidal mudstones to wackestones (see “Lithostratigraphy” section, this chapter). As seen in SSB A, SSB B is characterized by higher gamma-ray values (65–75 mbsf) than the background sediments.

SSB C, the Pleistocene/Pliocene boundary, corresponds to a depth of 160 mbsf (TWT) or 150 mbsf (Table 17). As in the two previous SSBs, this boundary can clearly be correlated to a high-velocity zone at or just above the boundary. Between 140 and 150 mbsf, the velocities suddenly increase from below 2 km/s to 4–6 km/s (Fig. 16). Lithologically, this high-velocity zone corresponds to the top of a thick, fine-grained, peloidal mudstone to wackestone that is capped at 138 mbsf by a bioclastic floatstone layer containing some blackened lithoclasts. Although low recovery does not allow reconstruction of the continuous record of the downhole velocity trend, the recognized high-velocity signature of the Pleistocene/Pliocene boundary probably results in the observed strong and coherent seismic reflection.

### Pliocene Sequences

The Pliocene Sequence *d* starts below 150 mbsf and probably forms the remainder of the drilled section. It consists mainly of peloidal mudstones to wackestones.

In conclusion, all three encountered SSBs (A, B, and C) are characterized in the cores by positive shifts in velocity and density and therefore by positive impedance contrasts. These signatures are likely to be caused by the combined effect of variations of lithology and diagenesis as a result of breaks in sedimentation. The concordance between the signatures in physical properties, lithostratigraphic boundaries, and hiatuses in sedimentation shows that the seismic data can resolve and image the distinct sequence-stratigraphic units in a carbonate slope setting.

## SUMMARY AND CONCLUSIONS

Situated at a water depth of 418.9 m on the western slope of GBB, Site 1004 was designed to (1) assess, in conjunction with other transect sites (Sites 1003, 1005, 1006, and 1007), the possibility of water movement through the marginal sediments of GBB, (2) provide a site for the study of high resolution sea-level changes during the Pleistocene, and (3) input additional information for the overlying sea-level objectives of Leg 166 (see “Site 1003” chapter, this volume). The 200-m-thick section of sediments recovered from Hole 1004A provides a record for the Pleistocene through the uppermost Pliocene, although the abundance and preservation of both nannofossils and foraminifers vary throughout the recovered sequence. The sedimentation rate is high throughout the Pleistocene, and modern platform production and shedding began to influence this site much earlier than the more distal site, Site 1003. For example, sedimentation rates increase from between 2.5 and 3 cm/k.y. at approximately 1.7 Ma at Site 1004 compared to 0.9 Ma at Site 1003. Based on comparison with Sites 1003 and 1005, only one lithologic unit was iden-

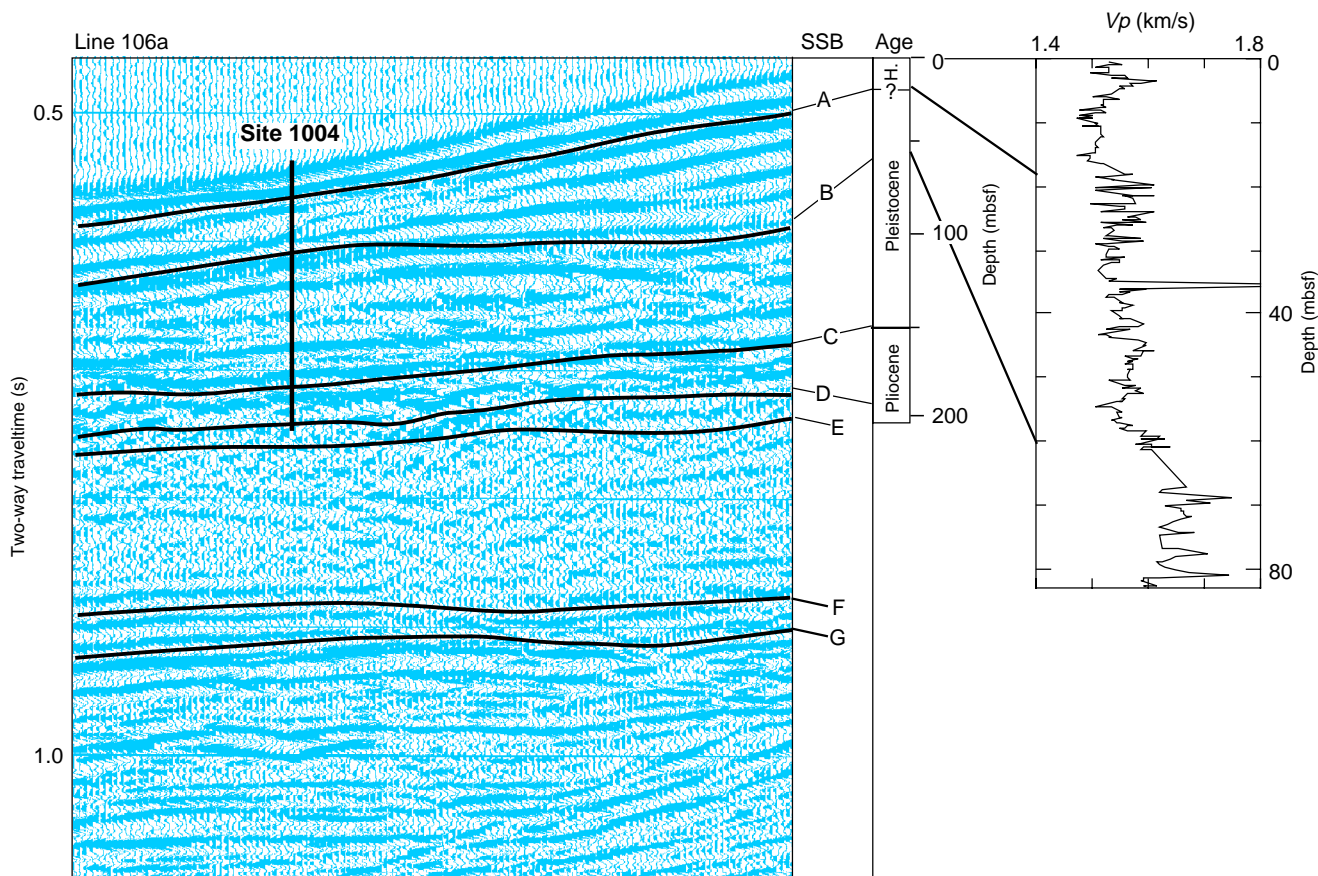


Figure 20. Part of seismic Line 106a with location of Site 1004. The seismic sequence boundaries (SSB) have been traced and converted to depth. All three SSBs coincide with downhole increases in velocity. The plot on the right displays the upper 80 m of velocity data where core recovery allowed continuous measurements.

Depth (mbsf)	Lith. unit	Seismic sequences	Biostrat. hiatuses	Age
0	IA	A a	No resolvable hiatuses	Pleistocene
		b		
		B		
		c		
		C		
100	IB	d	late Plio.	
		D		
		e		
200				

Figure 21. Correlation between lithostratigraphic units, seismic sequences, and biostratigraphic hiatuses and ages.

tified, which was subsequently divided into two subunits. Subunit IA (0–76.3 mbsf) contains multiple cycles composed of 10- to 15-m-thick intervals of light-colored unlithified to partially lithified peloidal wackestones to mudstones. These alternate with thin 0.5- to 1-m intervals of gray, partially lithified wackestones to packstones, grainstones, and floatstones. These variations probably relate to sea-level changes. Lowstands are characterized by a higher concentration of LMC and darker color, whereas the highstands contain abundant aragonite and HMC. Below the bottom of Subunit IA, these cycles can no longer be recognized as a result of poor core recovery and the in-

fluence of diagenesis, which results in the dissolution of aragonite and HMC and the formation of dolomite. Subunit IB (76.3–200 mbsf) contains an overall coarsening-upward sequence of partially dolomitized mudstones and wackestones with some coarser grained intervals.

In situ measurements using the Adara and WSTP tools indicate the presence of nonsteady state temperature profiles in the upper 40 mbsf of Hole 1004A. Below this depth, there is a uniform temperature gradient and heat flow. These profiles suggest either significant changes in bottom-water temperature over the past 100–200 years or the inflow of bottom water into the sediments. Input of bottom water is supported by the fact that there are no changes in the concentrations of either conservative ( $Cl^-$ ) or nonconservative ( $SO_4^{2-}$ ,  $Sr^{2+}$ ,  $Ca^{2+}$ , alkalinity) pore-water constituents over this same interval. Below the zone of uniform temperature and chemical composition, there is a steep change in the concentration of all chemical constituents. The concentration of  $Sr^{2+}$ , for example, changes from seawater values of 93  $\mu M$  at 40 mbsf to over 1500  $\mu M$  below 100 mbsf. Over the same interval, the  $Cl^-$  concentration rose from 559 to 680 mM. The absence of gradients between the seafloor and 50 mbsf clearly indicates that the upper 50 m of sediment is being flushed by seawater, although the precise mechanism involved is uncertain at the moment. The zone between 100 and 200 mbsf at Site 1004 is one in which there is abundant oxidation of organic material, causing complete depletion in sulfate, large increases in alkalinity, and abundant recrystallization of carbonate minerals. Water movement in this zone is postulated to be rather sluggish and the movement of ions controlled by diffusion, in response to different diagenetic reactions. This zone coincides with

**Table 17. Time-depth conversion and tentative age assignments of seismic sequence boundaries.**

Seismic sequence boundary	TWT below seafloor (msbsf)	Depth (mbsf)	Nannofossil zone	Foraminifer zone	Age	Age* (Ma)
A	20	15	NN21/20	N22	Holocene/Pleistocene	0.16
B	70	65	NN19	N22	Pleistocene	0.73
C	160	150	NN19	?	Pleistocene/Pliocene	1.7
D	200	185	NN18-16	N21	late Pliocene	2.6
E	220	Below TD				

Note: \* = ages are preliminary and based on shipboard biostratigraphy (see "Biostratigraphy" section, "Explanatory Notes" chapter, this volume).

high concentrations of CH<sub>4</sub> (up to 20,000 ppm) and H<sub>2</sub>S (up to 21,000 ppm). Although the C<sub>1</sub>/C<sub>2</sub> ratio is over 2000 in this region, there are still detectable concentrations of C<sub>3</sub> and C<sub>4</sub> present. These could be a result of in situ production or, alternatively, indicate the migration of these heavier hydrocarbons from an external source.

#### REFERENCES

- Baker, P.A., and Kastner, M., 1981. Constraints on the formation of sedimentary dolomite. *Science*, 213:215-216.
- Claypool, G.E., and Kvenvolden, K.A., 1983. Methane and other hydrocarbon gases in marine sediment. *Annu. Rev. Earth Planet. Sci.*, 11:299-327.
- Droxler, A.W., Bruce, C.H., Sager, W.W., and Watkins, D.H., 1988. Pliocene-Pleistocene variations in aragonite content and planktonic oxygen-isotope record in Bahamian periplatform ooze, Hole 633A. In Austin, J.A., Jr., Schlager, W., et al., *Proc. ODP, Sci. Results*, 101: College Station, TX (Ocean Drilling Program), 221-244.
- Droxler, A.W., Schlager, W., and Whallon, C.C., 1983. Quaternary aragonite cycles and oxygen-isotope record in Bahamian carbonate ooze. *Geology*, 11:235-239.
- Gaudett, H.E., and Lyons, W.B., 1980. Phosphate geochemistry in nearshore carbonate sediments: a suggestion of apatite formation. In Bendor, Y.K. (Ed.), *Marine Phosphorites: Geochemistry, Occurrence, Genesis*. Spec. Publ.—Soc. Econ. Paleontol. Mineral., 29:215-225.
- Gieskes, J.M., 1983. The chemistry of interstitial waters of deep-sea sediments: interpretation of deep-sea drilling data. In Riley, J.P., and Chester, R. (Eds.), *Chemical Oceanography* (Vol. 8): London (Academic), 221-269.
- Imbrie, J., Hays, J.D., Martinson, D.G., McIntyre, A., Mix, A.C., Morley, J.J., Pisias, N.G., Prell, W.L., and Shackleton, N.J., 1984. The orbital theory of Pleistocene climate: support from a revised chronology of the marine  $\delta^{18}\text{O}$  record. In Berger, A., Imbrie, J., Hays, J., Kukla, G., and Saltzman, B. (Eds.), *Milankovitch and Climate* (Pt. 1), NATO ASI Ser. C, Math Phys. Sci., 126: Dordrecht (D. Reidel), 269-305.
- Kastner, M., Elderfield, H., Martin, J.B., Suess, E., Kvenvolden, K.A., and Garrison, R.E., 1990. Diagenesis and interstitial-water chemistry at the Peruvian continental margin—major constituents and strontium isotopes. In Suess, E., von Huene, R., et al., *Proc. ODP, Sci. Results*, 112: College Station, TX (Ocean Drilling Program), 413-440.
- Kenter, R.J., 1985. Sea-level fluctuations recorded as rhythmic deposition in Northwest Providence Channel, Bahamas [M.S. thesis]. Miami Univ., Oxford, Ohio.
- Kier, J.S., and Pilkey, O.H., 1971. The influence of sea level changes on sediment carbonate mineralogy, Tongue of the Ocean, Bahamas. *Mar. Geol.*, 11:189-200.
- Kitano, Y., Okumura, M., and Idogaki, M., 1978. Uptake of phosphate ions by calcium carbonate. *Geochem. J.*, 12:29-37.
- Kohout, F.A., 1966. Submarine springs: a neglected phenomenon of coastal hydrology. *Central Treaty Org. Symp. Hydrol. Water Res. Dev.*, 391-413.
- , 1967. Ground-water flow and the geothermal regime of the Floridian Plateau. *Trans. Gulf Coast Assoc. Geol. Soc.*, 17:339-354.
- Mackin, J.E., and Aller, R.C., 1984. Ammonium adsorption in marine sediments. *Limnol. Oceanogr.*, 29:250-257.
- Schlager, W., and James, N.P., 1978. Low-magnesian calcite limestones forming at the deep-sea floor, Tongue of the Ocean, Bahamas. *Sedimentology*, 25:675-702.
- Slowey, N.C., 1985. Fine-scale acoustic stratigraphy of Northwest Providence Channel, Bahamas [M.S. thesis]. Univ. North Carolina, Chapel Hill, NC.
- van Morkhoven, F.P.C.M., Berggren, W.A., and Edwards, A.S., 1986. Cenozoic cosmopolitan deep-water benthic foraminifera. *Bull. Cent. Rech. Explor.-Prod. Elf-Aquitaine*, Mem. 11.

Ms 1661R-107

**NOTE: Core description forms ("barrel sheets") and core photographs can be found in Section 3, beginning on page 377. Forms containing smear slides can be found in Section 4, beginning on page 831. Thin sections can be found in Section 5, beginning on page 849. See the Table of Contents for material contained on CD-ROM.**